AN ABSTRACT OF THE THESIS OF

Sirilath J. De Silva for the degree of Master of Science in Atmospheric Sciences presented on December 06, 1990.

Title: Statistical Relationships Between the Mesoscale Organization Of Convection, Precipitation And The Large-Scale Wind Fields During The GATE.

Redacted for privacy

Abstract approved: _____
Steven K. Esbensen

Data from the GARP Atlantic Tropical Experiment (GATE) was analysed in an exploratory manner to discover the characteristics of mesoscale organization of convection and it's relationship to large-scale wind profiles. Automated methods were developed to identify the convective cells and their linear organization. These automated methods use a median high-pass filter to identify enhanced cells and a simple pattern recognition technique to ascertain the linear organization between them. Due to the simplified nature of the algorithm, the whole data set of the 21 day period from the phase 3 of GATE was processed in an economical manner obtaining a large data base which was used in the investigation of clusters and other associated phenomena. The mesoscale organization of convective cells and the widespread areas of lighter precipitation associated with them showed expected characteristics and compared satisfactorily with previous results. A large fraction of the rainfall (64%) fell from the widespread area. The total precipitation had a correlation of 0.94 with the fractional area of the widespread and a correlation of 0.89 with the fractional area of the clusters. The widespread

precipitation had a correlation index of 0.97 with it's fractional area and the cluster precipitation had a strong linear relationship to it's area with a correlation of 0.99. These factors argue well for the parameterization of rainfall rate in tropical regions to a high accuracy by the area covered by organized convective cells and widespread areas. It was also seen that there was a good correlation with the number of clusters and number of cores with the total precipitation rate in a given area. These factors create a strong argument for identifying mesoscale systems consisting of convective cells and widespread precipitation as basic units of precipitation in tropical regions, having a characteristic life cycle of their own. The widespread and total precipitation showed very good correlation with upper-level vertical motion. Clusters tended to align parallel with the horizontal low-level wind shear and the degree of alignment appears to depend on the strength of the wind shear.

Statistical Relationships Between The Mesoscale Organization Of Convection, Precipitation And The Large-Scale Wind Fields During The GATE

by

Sirilath J. De Silva

A THESIS

submitted to

Oregon State University

in partial fulfillment of
the requirements for the
degree of

Master of Science

Completed December 06, 1990

Commencement June 1991

APPROVED:

Redacted for privacy

Professor of Atmospheric Science in charge of major

Redacted for privacy

Head of Department of Atmospheric Science

Redacted for privacy

Dean of Graduate School

Date thesis is presented December 06, 1990

Typed by researcher for Sirilath J. De Silva

ACKNOWLEDGEMENTS

I am very grateful to the guidance, support, teaching, encouragement and friendship of my major advisor Professor Steve Esbensen. Many hours of stimulating discussions, invaluable advise and comments made this a significant educational experience for me.

Special thanks go to Bob Mobly for his help in computer programming and graphics assistance. Special thanks are also due to Nimal Gamage for his helpful assistance in computer graphics and constant encouragement. My gratitude also go to all my Sri Lankan friends in Corvallis and also to my officemate Phil Barbour for their constant support and encouragement. Finally, I would like to thank my mother Silta De Silva for her tremendous support, love and encouragement.

The research upon which this thesis is based, was funded by the National Science Foundation (grant ATM - 8718475). The computational work was done at the Computer Facility of the Atmospheric Science Department, Oregon State University.

TABLE OF CONTENTS

LIST OF FIGURES

LIST OF TABLES

STATISTICAL RELATIONSHIPS BETWEEN THE MESOSCALE ORGANIZATION OF CONVECTION, PRECIPITATION AND THE LARGE-SCALE WIND FIELDS DURING THE GATE

1.0 INTRODUCTION

1.1 Motivation of the study

The major objective of this research is to contribute to the understanding of the mesoscale organization of cumulonimbus clouds and its relationship to large-scale tropical flows. We will show that bulk measures of mesoscale organization such as the area covered and precipitation rate of tropical cloud clusters are dominated by these structures. The analysis will confirm the notion that the clouds clusters are not isolated phenomena, but have a definite relation to large-scale flows. Finally, we will quantitatively demonstrate a statistical relationship between the linear organization of cloud clusters and large-scale wind shear.

The heat sources in the atmosphere are mainly due to latent heat release and radiative heating modulated by clouds. As pointed out by Arakawa and Chen (1986), clouds are not only the prime cause for the heating gradients that drive motion but are the consequence of the motion too. This relationship is of fundamental importance in understanding the dynamics of the atmosphere especially in the tropics where local changes of temperature due to horizontal temperature advection are small.

Mesoscale organization is not represented explicitly in most large-scale numerical models. It is often assumed that there is a well defined gap in the spectral domain and strong interactions between convective and cumulus scale clouds (Arakawa and Chen, 1986). Considering the convective clouds in a grid box to be statistically homogeneous may not be sufficient for describing

the effects of cumulus clouds in a large-scale numerical model.

Arakawa and Chen (1986) reviewed the principal types of cloud parameterization schemes that are currently being employed in numerical models. In the large-scale condensation scheme, mixing ratio and the temperature are continuously adjusted to the equilibrium saturation state when various processes tend to make them super-saturated. This scheme is suitable for the parameterization of anvil clouds or large upper-level cloud layers where the motions giving rise to condensation and evaporation are explicitly resolved by the model. The relationship between advective forcing and cloud response can be obtained directly, and the advective process alone determines the net warming and moistening. In the moist-convective adjustment scheme, the vertical distribution of net warming and moistening are completely determined by the closure assumptions on the lapse rate and mixing ratio. In Kuo's scheme, the mixing ratio and temperature of the cloud model is taken to be at an equilibrium state lying on a moist adiabat. In this scheme there is no dependence of the vertical structure of the heating on the advection process; the vertical distribution of net moistening and heating are completely determined by the respective deviations of the temperature and mixing ratio from their equilibrium states. The modified Kuo scheme applies to unsaturated cases and partitions the effects of advective processes between net warming and moistening. The Arakawa-Schubert scheme introduces a cloud work function that takes into account a population of cloud types. This scheme, which is basically a convective adjustment scheme where the adjustment is done by comparing the cloud-type dependent work function with it's critical (minimum) value. The above given classical schemes differ from each other by the closure assumptions used and also by the details of the formulations but none of them explicitly represents effects of mesoscale

organization.

Houze and Betts (1981) in their work on convection in GARP (Global Atmospheric Research Program) Atlantic Tropical Experiment (GATE), came to the conclusion that mesoscale organization of tropical convection should be considered in large-scale models. In addition to convective scale updrafts and downdrafts, features such as anvil clouds with middle tropospheric mesoscale convergence patterns and mesoscale updrafts at upper levels and downdrafts at lower levels appear to play a key role in thermodynamic and dynamic structure of the large-scale environment. Therefore to successfully parameterize momentum, heat and moisture distribution in convection we must study mesoscale systems to understand the quantitative importance of these features.

The interaction of large-scale flows with cloud organization has not been widely studied in theoretical and numerical literature. This is primarily due to the lack of a physical and mathematical framework in which the clouds and large-scale flow, which span a wide range of spatial scales, can be quantitatively described. Clouds involve complex physical processes such as downdraft forcing due to rain drag and evaporation, conversion of cloud water to rain, interaction of updrafts and downdrafts etc. The fact that the latent heat release and the condensation vary vertically in a complicated manner has acted as an impediment to the work in this area.

Understanding all of these physical processes is therefore of immense importance in the cloud parameterization schemes used in numerical models. It is apparent that the cumulus updrafts are not isolated phenomena, but are entities of larger cloud organization with associated mesoscale motion fields with a strong interdependent relationship. Therefore the knowledge of these relationships would be of importance in developing and verifying the

parameterization schemes.

1.2 Theoretical studies of cloud organization

In the theoretical studies, researchers have generally employed simplified equations of fluid dynamics to study the cloud organization. Their work has been centered on linear stability analysis and numerical modeling to ascertain the conditions that are favorable for this organization.

Asai (1970) investigated the behavior of convective perturbations of Couette flow neglecting latent heat release. Numerical methods were used to solve a linearized quasi-Boussinesq set of equations in which the effects of latent heat were ignored. Asai's study was based on the dynamical structure and the energy conversion process for two types of convection; one that is oriented across the mean flow - the transverse type - the other along the mean flow - the longitudinal type. He examined the amplification rate and stability of the perturbations as functions of the Richardson(Ri) number and the horizontal wave number of perturbation. He concluded that large vertical shear favored the development of lower-wave-number modes, and lesser vertical shear that of higher-wave-number modes. The dynamical reasons could be deduced by observing the vertical profiles of temperature and vertical velocity for the two cases. For the case of lower-wave-number, the conversion of potential energy to perturbation kinetic energy was favorable. It was also observed that, even though the maximum amplification rate shifted to lower-wave-number with lowering of the Ri number, the maximum value itself diminished and the value below a certain cutoff value was zero . Another observation was that longer wavelength perturbations (low-wave-number) had a clear preferred mode while the amplification rate for the shorter waves did not vary much with the wave number. By studying the phase velocity of the

perturbations it was also seen that the longer modes were stationary while shorter ones propagated with respect to the mean flow.

To ascertain the sensitivity of the growth of the perturbation on its structure, Asai (1970) examined the equation for the kinetic energy of perturbations. Asai found that the rate of increase of the kinetic energy of perturbation depended on the conversion of mean potential energy and mean kinetic energy of the flow to perturbation kinetic energy minus that due to viscous dissipation. Also the mean kinetic energy conversion process was found to play a crucial role in determining the structure of the convective process as will be explained later. In studying the vertical profiles of the vertical transport of heat it was apparent that the contribution to the growth of the kinetic energy of perturbation by the conversion of potential energy was positive at all levels and the direction of the conversion was independent of the orientation of the perturbation. In contrast it was seen that the vertical transfer of horizontal momentum is upwards against the shear for the transverse case and downwards for the longitudinal case. It was also seen that larger momentum transfers occurred with lower Ri number by considering the ratio between the volume average of the two terms - the conversion of mean available potential energy to perturbation kinetic energy and the conversion of kinetic energy of mean flow to perturbation kinetic energy.

Additional physical insight was obtained by examining the structure of the perturbations. In the case of transverse perturbations, the vertical velocity and horizontal velocity patterns were found to be in phase and the flow streamline patterns tilted with height in the direction of shear. This behavior is entirely consistent with the results of two-dimensional convection which intensifies shear by the vertical transfer of momentum. For the case of longitudinal perturbations it was seen that the vertical velocity and hori-

zontal velocity patterns were out of phase and the flow streamline patterns tilted with height against the shear. The reason for this tilt was hypothesized using the vertical component of the vorticity equation. It was deduced that the three-dimensional flow pattern of the longitudinal mode brings about vortex tilting from horizontal to vertical due to the variation of the vertical velocity in the transverse direction. It was inferred that this flow pattern structure was responsible for the transfer of kinetic energy of mean flow to the perturbation kinetic energy.

Asai (1970) concluded that the linear vertical shear has a stabilizing effect on the perturbations of the flow. The effect is more pronounced for short wavelength perturbations for both transverse and longitudinal modes, as well as perturbations that have a longer wave length across the mean flow. In both cases the kinetic energy of perturbation was increased by the conversion of potential energy associated with the upward transport of heat. In the case of transverse disturbance, part of the perturbation kinetic energy was converted to the mean flow kinetic energy while in the longitudinal case mean flow kinetic energy was converted to perturbation kinetic energy. Thus it was evident that the longitudinal mode was the favored mode for convective disturbances. Another interesting result was that the magnitude of the energy conversion between mean flow and the perturbation kinetic energy was inversely proportional to the Richardson number. Thus it was inferred that a large wind shear favored the longitudinal mode of convection due to larger conversion of energy from mean flow to perturbation kinetic energy. A similar argument held for the suppression of the transverse mode of convection, because in that case the energy conversion was from perturbation to mean flow kinetic energy thereby draining away the perturbation kinetic energy.

Sun (1978) considered the combined effect of latent heating and wind shear in the tropical atmosphere in an attempt to explain the mesoscale cloud observations by Malkus and Riehl (1964). Compared to Asai's (1970) study, this was more realistic because of the consideration of latent heat release. In his study, Sun assumed that the convective bands were driven by the released latent heat in a stably stratified atmosphere with a mean wind shear. The numerical model used in the study was based on an atmosphere bounded by two sliding horizontal planes separated by a distance of 16km to account for the vertical scale of motion. Mean-state density was taken to be related to height only, the Coriolis force was neglected and the atmosphere was taken to be anelastic for simplicity. It was found that if the buoyancy force created by the release of latent heating is stronger than that of damping due to static stability, then the cloud bands will form parallel to the wind shear and be stationary with respect to the mean flow. But, if the buoyancy force is weak, then the conversion of kinetic energy from the mean flow dominates and the bands become perpendicular to the wind shear (transverse mode), propagating relative to the mean flow.

To study the influence of the height of the cloud top on the organization, Sun (1978) varied the height from 5.6km to 10.4km. The reason for selecting this range was that for a cloud top hight below 5km would bring in the possibility that the latent heat release may not be proportional to the moisture convergence for very shallow clouds, and the cloud top hight above 12km would force the consideration of interactions among deep clouds. In the model the heating within the cloud was represented by a function that depended on the cloud height. It was observed from the model that for the shallow clouds the preferred orientation was longitudinal bands while that for deep clouds it was transverse bands. This was interpreted from a point

of view of energetics. For the shallow clouds the potential energy released by the buoyancy force was larger than that of the conversion of kinetic energy of perturbation from the mean flow, thereby making the flux Richardson number considerably larger. This was due to the latent heating effect being larger than cooling or damping effect due to stable stratification. Looking at the relationships of the growth rate, wave number and orientation angle for different flux Ri numbers, it was seen that for higher numbers the growth rate was not sensitive to the orientation of the bands. Thus even though the shallow clouds preferred longitudinal bands, they were not strongly selected. For the deep clouds the opposite was true. There the cooling or damping effect was comparable in magnitude to the diabatic heating, thereby reducing the importance of the buoyancy term. Thus the wind-shear production term can dominate the buoyancy term. Therefore the deep-cloud growth rate was sensitive to the orientation, and the transverse bands efficiently convert mean-flow kinetic energy to the perturbation.

The sensitivity of the model to the details of the cumulus parameterization scheme were checked by varying the ratio of horizontal moisture convergence to condensation of moisture in clouds. The sensitivity was also checked by comparing a diabatic heating function that was sinusoidal in nature within the cloud with another that was close to the observed diabatic heating difference between trough and ridge areas. No marked sensitivity to these differences in the parameterization of heating by the unresolved convection were found.

To check the sensitivity of the model to the details of the wind profile, two profiles were used. One had its direction constant but the magnitude changing with the height as observed in easterly-wave trough regions, while the other had constant speed but with rapidly changing direction in a shallow

layer in between two uniform flow layers at levels of 4km and 7.2km. It was observed that these changes in the wind profiles did not have a marked influence.

Thus it was deduced from the model that in a moderately disturbed trough region, the deep clouds will form cloud bands in the transverse mode while medium-size shallow clouds will form bands in the longitudinal mode. Sun concluded that the propagating frequency and growth rate of deep cloud streets is governed by the moisture supply, the strength of the wind-shear, static stability and viscosity. The orientation of these bands depended on the relative strength of the buoyancy force to that of static stratification. As an example, large convective heating can enable the buoyancy force to overcome stable stratification brought about by damping which is dependent on cloud top height. Similarly the moisture convergence can also enhance the diabatic heating term so that the buoyancy term is increased. These factors can allow the buoyancy term to dominate the shear production term, thus creating the possibility that deeper clouds may prefer longitudinal mode.

Using both analytical and numerical methods, Moncrieff and Miller (1976) studied the structure of tropical cumulonimbus both analytically and numerically, using a quasi-Boussinesq three-dimensional model. For the growth, development and maintenance of deep convection, they found that the thermodynamic and kinetic states of the large-scale flow were both of major importance. This model simulated the linear organization of the squall lines (transverse mode) well. They concluded that the propagation speed of the cumulonimbus depends on the convective available potential energy of the basic state, and weakly on the bulk Richardson number. Thus it is seen that there are specific large-scale parameters which can be used as an indication of the possibility of this type of linear organization.

In contrast to the transverse squall lines studied by Moncrieff and Miller (1976), Tao and Soong (1986) studied well-defined longitudinal Inter Tropical Convergence Zone (ITCZ) rainbands over the GATE area. Their studies involved cases with low wind shear and had Ri number greater than 2.8. Another obvious difference was that the squall lines propagated with respect to the mean wind but the rainbands were more or less stationary. In their study Tao and Soong performed numerical model studies of convective clouds using a model that was non-hydrostatic and anelastic, with Kessler's (1969) parameterization scheme for cloud microphysical processes. Temperature perturbations were found to be necessary to maintain the horizontal inhomogeneity of the atmosphere produced by the large turbulent eddies in the boundary layer. It was seen that the amount of precipitation was very sensitive to the imposed large-scale rising motion, and the large-scale temperature and moisture fields were sensitive to changes in the parameterization of micro-physical process. The simulated clouds in the model formed cloud bands in all the cases studied except for the case without wind shear. In the latter case the simulated clouds developed randomly and had short lifetimes. In agreement with observations, they found that the cloud bands were aligned along the lower tropospheric wind shear. The simulated cloud bands propagated slowly normal to their major axes (and the mean shear vector), but the individual convective cells propagated much faster in the direction parallel to the bands.

In another important work Dudhia and Moncrieff (1987) simulated ITCZ cloud bands with a numerical model that is a modified version of the Miller and Pearce (1974) three-dimensional convection model. Unlike Tao and Soong (1986) who studied organized mesoscale clusters by applying their three-dimensional model to a case of well defined ITCZ band over the east-

ern tropical Atlantic, Dudhia and Moncrieff (1987) initialized their model with the wind and thermodynamic data from the GATE. They showed that the convective bands that are aligned with shear, in contrast to squall lines, have a lesser influence on the large-scale momentum. This is due to the fact that the squall lines have a higher mean flow kinetic energy available to them due to their perpendicular alignment with the wind-shear which results in large eddy momentum transport. Convective bands parallel to the wind shear will be more effective in mixing of easterly momentum and will have a different dynamical structure due to their 3-dimensional nature. In this case, the low-level easterly jet was found to deviate around the band but some easterly momentum was transferred to the updrafts by the pressure gradient force; some momentum was also transferred downwards by the descent of jet air due to rain drag and evaporation.

In the case of moisture and heat, Dudhia and Moncrieff (1987) found that quasi-stationary bands influenced the large-scale environment by warming and drying mainly due to mid- and upper-tropospheric subsidence; cooling and moistening of the environment from the cloud evaporation at the jet level and at the cloud top; warming and moistening from the anvil cloud near the 400mb level and cooling and drying at the surface by the downdraft flows. Also due to the 3-dimensional nature of the bands that are aligned with wind shear, the air detrained from updrafts will possess a considerable amount of vorticity due to vortex tilting. Thus there will be organized turbulent mixing downstream of the updraft cores which enhances rapid evaporation of clouds thereby cooling and moistening the environment.

One of their conclusions was that the GATE soundings used were sufficiently destabilized that even a weak large-scale upward motion could initiate substantial mesoscale systems. Using sensitivity analysis they also concluded

that the growth and sustenance of organized cumulonimbus cells were dependent upon the strength of the forced large-scale mass convergence at lower levels. This mass convergence provided a moisture and hence a latent energy supply. The mean ascent due to convergence at low-levels created adiabatic cooling in and above the surface convergence layer thereby increasing the potential instability. Therefore the updrafts were strengthened in this lifted environment and the low-level convergence maintained the moisture supply, thus enabling the convective instabilities to persist by opposing the warming and drying effects of clouds on the environment. In the model simulation they also observed that the alignment of updrafts parallel to the shear, protected the cores from being mixed with the environmental air at the level of the mid-tropospheric jet stream. The convective band that was simulated was longitudinal and therefore different from the transverse squall lines simulated by Moncrieff and Miller (1976). Dudhia and Moncrieff concluded that the simulated system was similar to bands observed during GATE and that the strong low-level shear played a key role in the development and orientation of the bands. Thus it is seen that there is a theoretical and an experimental base for the relationships between the upper-air wind data and the concurrent radar reflectivity data from the Phase 3 of the GATE.

1.3 Observational studies of cloud organization

The stochastic nature of the clusters and the echo cores that constitute them have been studied by Houze and Cheng (1977), Raghavan et al (1983) and others. A case for this stochastic nature can be based on the fact that the conditions favorable for the convective activity may be present for a long time, but the individual mesoscale cloud features will grow or decay due to the exhaustion of the local supply of moisture and heat sup-

ply from the sea surface during their life-times. Clusters may also merge or break-up. Therefore it is evident that the favorable synoptic conditions by themselves will not generate the mesoscale precipitation features. The stochastic nature has also been reinforced by the observation of log normal distribution of convective cores' sizes. This has been explained by the well accepted argument that favorable conditions bring about convective cores which act as seeds which grow by entraining environmental air in some proportion of the initial mass. The stochastic nature of analysis is also based on the studies done by Houze and Cheng (1977) and other researchers who all accepted the notion that the relationships have a more of a statistical basis than a deterministic one. As explained by Houze and Betts (1981) large-scale flow features such as Hadley cells, synoptic-scale waves, diurnal variations and outflow from previous convective systems influence the cloud patterns. Therefore a stochastic representation would be more realistic than a deterministic one. The stochastic nature of the convective clouds necessitate looking at statistical relationships of clusters with large-scale flows and the general characteristics of a representative cluster.

From the work done by Dudhia and Moncrieff (1987) and other theoretical work indicated above, it is known that the large-scale forcing is necessary for the maintenance of quasi-stationary convective lines formed over the ocean. Therefore it would be natural to look for statistical relationships between organized mesoscale precipitation features and large-scale divergent motion.

Another obvious area to examine is the orientation of the cloud bands with respect to the wind shear of large-scale wind flows. This relationship has important dynamical implications since cloud bands oriented parallel to the shear are likely to have much different internal pressure and momentum

fields in comparison with cloud bands oriented normal to the wind shear. Therefore the organization would be of importance in determining the effects of clouds in the large-scale momentum budget.

As shown by Leary and Houze (1980) a large mesoscale system with an area on the order of $20 \times 10^4 \text{km}^2$ can have characteristic divergent motion field of it's own. This field is composed of a relatively small convective area with updrafts and downdrafts drafts, and a larger mesoscale region with updrafts at higher levels and downdrafts at very low-levels. The mesoscale cloud systems have a marked contribution to the vertical profiles of large-scale wind and thermodynamic variables and therefore are of great importance in parameterizing the effects of convection on the large-scale environment. As explained by Houze and Betts (1981), a large proportion of the precipitation comes from the anvil clouds in the mesoscale convective systems which accounted for 90% of the precipitation in GATE. These mesoscale systems have complicated motion fields with strong convective scale updrafts in the initial stage. The mature stage and dissipation stages are characterized by the mesoscale ascent at upper levels and downdrafts at lower levels. In their study they also came to the conclusion that the total precipitation amount and large-scale vertical motion were coupled. Thus the importance of the motion field in the parameterization of the transport of heat and moisture flux for coarse-resolution numerical models is apparent.

Each type of mesoscale organization, either transverse or longitudinal, has a different motion field. Is the relative frequency of occurrence of these bands high enough to be of significance to the large-scale dynamics? If so, parameterization schemes for clouds in numerical models of the large-scale flow over tropical ocean would need to have a representation of mesoscale motions in addition to the effects of convective motions. To answer these

questions and to gain a knowledge about these systems a study oriented towards these problems is of paramount importance.

There are very few quantitative, observational studies of mesoscale cloud organization and its relationships to the large-scale flow over the tropical oceans. The pioneering work of Malkus and Riehl (1964) described organized mesoscale cloud patterns observed during aircraft flights over tropical Pacific. They found that shallow convective clouds were mostly organized into longitudinal rows or bands, while the deep clouds were organized into bands of a variable nature, being either transverse or longitudinal. It was also observed that cloud streets developed in the area where the wind direction was almost constant in the convective layer, or where the wind speed remained constant with height but the direction changed rapidly in a shallow layer between a rather uniform flow in a deep layer above and a rather uniform flow in the cumulus layer below.

A case study of deep cloud organization during GATE has been presented by Warner et al (1980). Clouds which penetrated into the middle troposphere appeared to be aligned along the direction of wind shear in the lower troposphere. Deep clouds which penetrated to the 15km level appeared to be related to the surface confluence lines which were determined from low-level satellite-observed cloud movement. Warner et al (1980) studied a single day (day 261) of GATE with a goal of gaining more knowledge about cloud clusters. He observed that the clouds in this particular day had an organization similar to that of the theoretical studies done by Sun (1978) in which linear organization parallel to wind shear was preferred for situations where buoyancy forces were stronger compared to the damping effect due to stable stratification. Case studies of this nature are comprehensive studies of a specific event involving convective activity. Thus a detailed picture of the

mechanism involved in organizing convection for selected events could be obtained. But it should be kept in mind that there are weaknesses in case study approach. They are being the limited number of cases that can be examined and the question whether a conclusion based on this small number of cases could be generalized to every situation.

Using manual identification methods, Houze and Cheng (1977) identified cloud clusters from the GATE reflectivity data. They grouped the clusters into different area-size categories, and then used simple statistical methods to study each category. These statistical results gave a certain idea about the life-cycle of the clusters, the area coverage of it and a tool to compare with other researchers who also have employed manual methods to identify clusters. In their study they also found that the linear organization occurred in approximately 80% of the cases and of these approximately 80% of cloud lines or bands were within $\pm 25^{\circ}$ of the 700mb or 800mb wind direction. However the quality, areal coverage and resolution of their wind data was limited in comparison with the total information available. Only data near 1200GMT were analysed. Lopez (1978) also extensively used manual methods to pick clusters from radar pictures and computed certain basic statistics about them. It is evident, that from these manual methods general characteristics of the clusters could be evaluated, but it would be of labor intensive in nature.

A similar manual identification of mesoscale organization was done by Houze et al (1990). In this case they studied major rain events in Oklahoma. Here they were able to categorize the organization according to the degree of conformity to a idealized model of leading-line/trailing stratiform structure and the symmetricity of the structure. By this method they were able to have a large number of classes and study each one separately. One of

their conclusions was that about two-thirds of the cases had a distinct linear organization.

Crane (1990) in his studies of High Plains Experiment data, observed that in storms the convective cores had an average separation distance of 12km. He hypothesized the rain process as two dimensional turbulence with the energy needed to drive it obtained from mesoscale convection. In another study Ramirez and Bras (1990) studied the statistical character of observed and simulated cloud fields. They came to the conclusion that due to the intrinsic nature of the convection process the clouds formed regular patterns as opposed to totally random distribution.

To explore these ideas and relationships in a systematic and quantitative manner, we have developed automated techniques to process the data from the GATE Phase 3. Due to the enormous amount of data, automated techniques were the logical choice. One of the main tasks in the systematic exploration of cloud organization using automated techniques is the identification of intense cells or cores from the widespread areas of precipitation. A basis should be devised that would give a fairly accurate representation of cores or intense cells from the surface precipitation data. The method should be robust enough so that it is stable for small observational errors in the data field and should also be insensitive to edges in the data field and missing data. Once the intense precipitation cores have been identified the next step involves recognizing the spatial patterns formed by the intense cores. For this step an algorithm is needed that recognizes the patterns among the cores. The specific pattern which is of interest here is a set of cores with a linear structure. After finalizing the methods for doing the crucial steps, as outlined above, the automated techniques can be employed for the systematic exploration of the cloud organization using the surface

precipitation data.

The knowledge that can be gathered from this exploratory study are the area covered by various components of the cloud systems, the spatial distribution of the components, the degree of linear organization of cloud features, the orientation of cloud bands with respect to the wind shear, and the precipitation amount in cores and cloud systems as a whole. Statistical evaluation of the above mentioned parameters will impart certain amount of understanding about the organized precipitation cores and, by inference, organized convective systems.

Looking at the advantages of the automated techniques, it is evident that they can be fast and efficient. Thus they would have the ability to process a large amount of data, thereby facilitating a large sample of data for statistical study. This is a particular advantage when one wishes to explore various criteria in the identification of the cloud organization.

Automated methods do have disadvantages, however, due to the requirement that the methods be simple and fast. Our pattern recognition methods consist of a few basic objective steps, and cannot handle complicated structures of cloud organization, or track their evolution with time. Manual methods depend on the complexity of human judgment to identify complicated features and can overcome most of the failures of the automated methods. This superiority of manual methods is based on the ability of the human mind in judgement and recognition of patterns. Thus the manual methods will have the advantage of being able to handle complicated structures of cloud organization and assign a orientation and a linearity to it in an acceptable manner. For example, patterns that have complicated structures with branches in different directions may have a specific orientation that could be evaluated easily by human judgement, but could be assigned

a totally different direction by the automated methods. Also by subjectively evaluating the data field in manual methods, we would be able to identify the spurious and missing data in the data field more easily.

The disadvantages of the manual methods are in the limitation in speed and variations due to subjective judgments by different researchers. Therefore it will not have the uniformity of automated methods. Another disadvantage is the bias towards the expected results by the human evaluator. The time consuming nature of manual methods would also be a disadvantage as it would obviously limit the amount of data that could be processed. Most previous studies of mesoscale cloud organization can be categorized as either case studies or manual identification methods.

2.0 DESCRIPTION OF METHODS OF CLUSTER IDENTIFICATION AND STATISTICAL ANALYSIS

In this chapter we describe the methods and data used to identify cloud clusters and to evaluate their relationship with the large-scale flow. The primary data sets are analyzed fields of upper-air wind from conventional sounding data, and precipitation estimates from meteorological radar. Statistical and exploratory data analysis methods were utilized to find the characteristics of the clusters and associated phenomena.

A basic understanding of convective cells is obviously of importance for the proper understanding of clusters. A cluster is identified by enhanced precipitation cores which we will associate with convective cells characterized by strong updrafts and downdrafts. Each cluster is made-up of one or more mesoscale precipitation features (MPFs; see Houze and Betts, 1981). These MPFs have strong convective cells embedded in weaker widespread areas of convection which correspond to mesoscale anvil clouds or dying stages of convective cells. These mesoscale convective systems can form over ocean or over land. As summarized by Houze and Betts (1981) for GATE, it was seen that most of these systems over the ocean are slow moving bands of convective cells with associated widespread areas of precipitation from stratiform clouds composed from the anvil clouds. Compared to the continental systems, convective cells over the ocean are characterized by relatively small updraft velocities and a rapid decrease of reflectivity with height. Szoke et al, (1986) suggested that the reasons for this are the relatively low Convective Available Potential Energy (CAPE) over the ocean and the high liquid loading brought about by the marine environment enhancing the rapid growth by coalescence.

The radar data used in this project were obtained using the C-band (wavelength 5.3cm) radars aboard ships during Phase 3 of GATE. The radars had a range of 256km and a complete set of scans was obtained every 15 to 30 minutes in the volume above the ship by changing the vertical tilt angle of the radar in increments and sweeping in 360° horizontal arcs. The reflectivity data from the radars were converted from the polar form to Cartesian hybrid plan-position-indicator format. The Cartesian arrays of 4km×4km data bins contain mean equivalent reflectivity data averaged over the grid area in dBZ units with resolution of 1 dBZ. The dBZ unit is given by ten times the base-10 logarithm of the radar reflectivity factor. This factor and rainfall rate are related by an empirical relationship (Patterson et al, 1979).

As explained in Patterson et al (1979) the radar data were quality-controlled using manual and automated schemes. One way this was done was by inspecting the microfilms and eliminating bad scans. The contamination due to sea clutter was minimized by compositing digital hybrid scans using annuli from the scans of the lowest three tilt angles of the antenna for three out of four ships of the GATE experiment, namely Gilliss, Researcher and Oceanographer. These hybrid scans were used to eliminate the sea clutter contamination of the data from all except the four Cartesian grid boxes surrounding the ship center. For these center grid boxes an objective analysis model was used to fill in the data.

The conventional data which comprised upper-air data for this study, were obtained by optimum interpolation of wind over the A/B and B ship arrays during Phase 3 of GATE. The analysis scheme (see Ooyama, 1987) was formulated in such a manner that it would create from the wind data a horizontal wind field which would have all the information on space and time scales of the soundings but would minimize undesirable effects of temporal

and spatial aliasing. The scale of large-scale flows are of meso-α scale, which is comparable to the scale size of large cloud cluster thereby enabling the study of interaction between cluster and the motion field using this data set. The data from the wind analysis is archived on a $9° \times 9°$ latitude and longitude grid centered at 8.5°N and 23.5°W. A grid interval of 0.5° in latitude and longitude is employed which gave a 19×19 array. This data array is computed for each 41 constant pressure level from near the ocean surface (1012mb) to 70mb level. The analysis was performed for each 3 hour interval during the GATE Phase 3 time period of 30 August to 18 September 1974.

2.1 Determining the mesoscale organization

As an initial step in analyzing the mesoscale organization of clouds during the Phase 3 of GATE, the radar echo data from the ship Gilliss were obtained from the National Climatic Center, Ashville. These radar data consist of horizontal Cartesian grids with 4km×4km resolution within a radius of 256km at 15 to 30 minute intervals during the 18 day period of 31 August - 17 September 1974. The upper-air data used has uniform coverage in space and time for the 18 days during Phase 3 of GATE as described above. The combination of the upper-air data with radar data provides a unique opportunity to statistically examine the tropical cloud organization and its relationship to the large-scale flow.

2.2 Methodology used for automated cluster identification

The radar reflectivity signals from the precipitating clouds on each 15 minute scan were first broken into connected sets of echoes with non-zero

dBZ values which we have called "groups". To separate the enhanced precipitation cores of intense convective cells from the rest of the background precipitation, a high pass filter was applied to the dBZ values. This was in the form of a moving median filter of 36km x 36km area. Each echo group was processed independently; i.e., the value of the reflectivity for a point that is not a member of the group is assumed to be zero. The filtering was done by moving the filter window over the data in the group and then computing the median value of all the data that fell within it at each position of the window. The dBZ value at the center of the filter window is replaced by the median value. The size of the filter window determines the response of the filter, and was designed to remove deep convective cells and other small-scale atmospheric phenomena, thereby leaving the environmental values.

The median filter has some important advantages over linear filters. It is simple and reasonably efficient, and is able to completely filter out isolated, small-scale precipitation features that would produce a significant response for a typical linear convolution or recursive filter. The other advantage is the median filter's insensitivity to magnitude of the rainfall. Any monotonic function of rainfall rate will give the same result. This gives the practical advantage of being able to perform computations using dBZ values which are economical to represent and store.

To identify the grid boxes which constitute intense cells of precipitation, it was assumed that a cell must have a precipitation rate that is 5mm/hour greater than its environment. The choice for this cutoff is somewhat arbitrary. From a subjective viewpoint this choice gives a good identification of the intense cells. This fact is illustrated by the Figs. (2.2.1a) to (2.2.1c). Here a scan from the Gilliss on day 248 is processed by the automated method to identify the grid boxes which constitute the intense cores, with varying

cutoff values of 3, 5 and 7mm/hour. The grid boxes of interest are demarcated by the inscribed squares given by the black outline. It is apparent from the figures that in the case of 3mm/hour the method picked-up cells that were not very intense while in the case of 7mm/hour it failed to identify some of the intense cells. In the 5mm/hour cutoff case results appeared to identify intensely active regions and produced stable statistics. Therefore the cutoff value of 5mm/hour was chosen as our criteria for identifying the intense precipitation cores.

Figure (2.2.2a) and Fig. (2.2.2b) give the frequency distributions of the dBZ values in all the scans for widespread areas and cores. Figure (2.2.2a) considers the dBZ distribution and Fig. (2.2.2b) considers the precipitation contribution by each interval. It is apparent that the 5mm/hour cutoff resulted in the number of grid boxes that constituted the cores being small with respect to widespread areas, but when the precipitation contribution is considered it is seen that it is substantial. From the overlap in the cores and widespread area cells in both the figures it is clear that this method differs from plain threshold methods such as the one utilized by Atlas et al (1990).

The echo cores or intense cells were defined by a set of one or more grid boxes having large precipitation rates in comparison with their surroundings. Clusters of echo cores were identified using the single-linkage cluster analysis technique of Gower and Ross (1969). This was done by constructing a minimum spanning tree linking the positions of the intense cells in the scan. To isolate the clusters of cores, links greater than a distance cutoff of 24km were removed from the minimum spanning tree. This choice of cutoff was justified by the fact, that it is roughly twice the scale size of the cumulonimbus cloud, and any cores separated by a distance more than this could be thought as having little direct influence on each other.

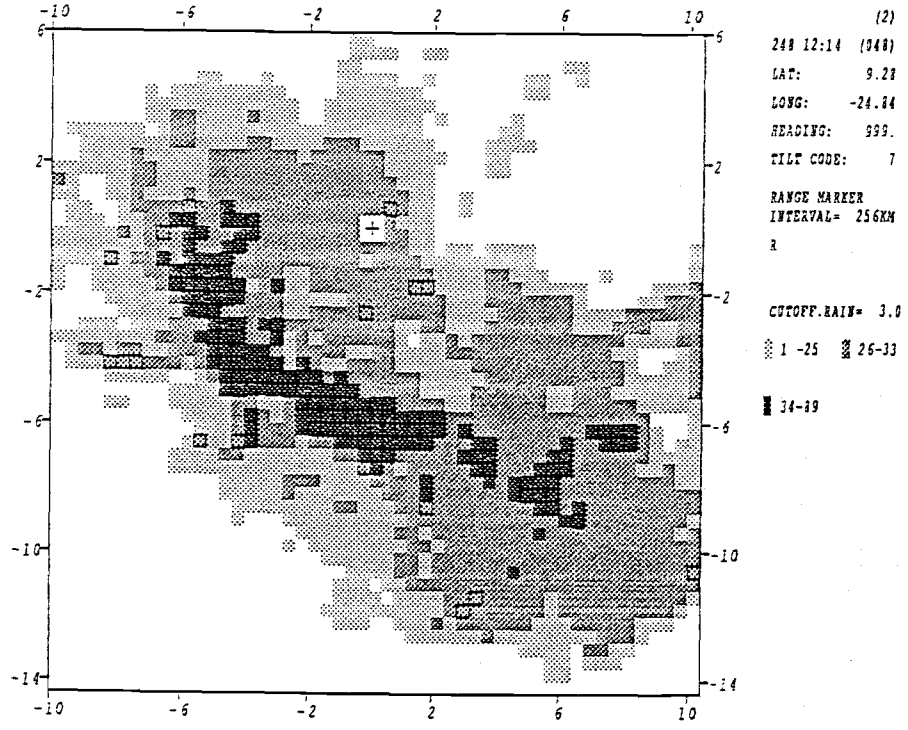

Fig. (2.2.1a) Day 248 scan section with 3mm/hour cutoff

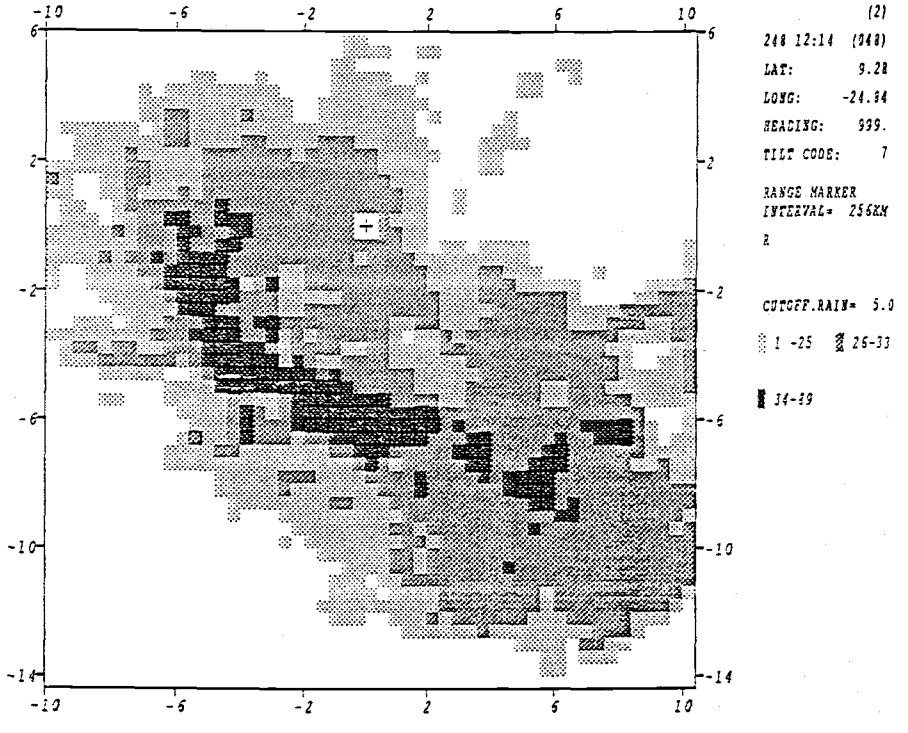

Fig. (2.2.1b) Day 248 scan section with 5mm/hour cutoff

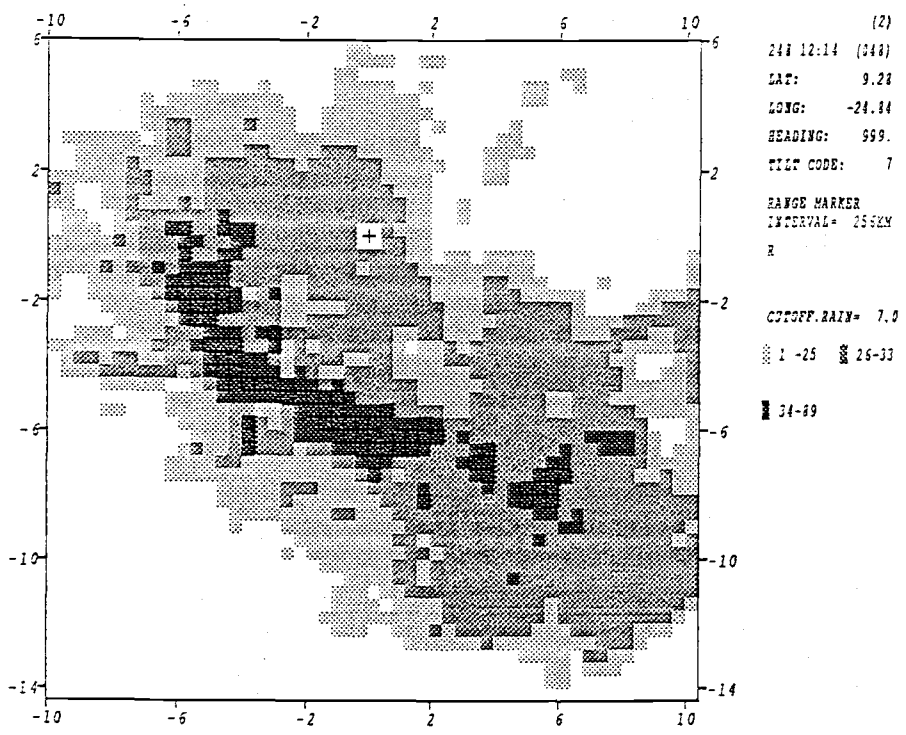

Fig. (2.2.1c) Day 248 scan section with 7mm/hour cutoff

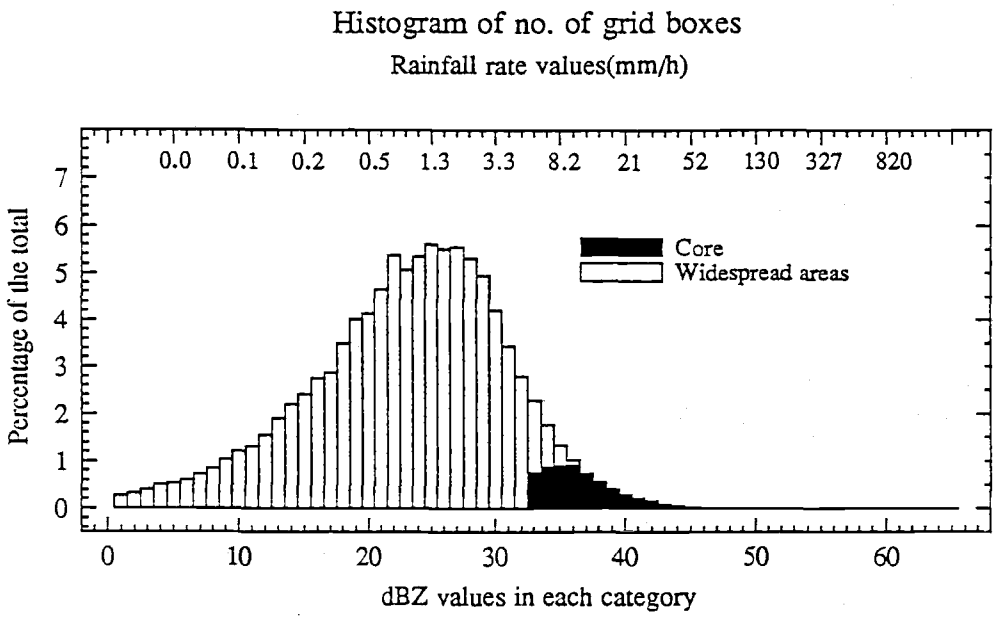

Fig. (2.2.2a) Frequency distribution by the number of cases in each interval

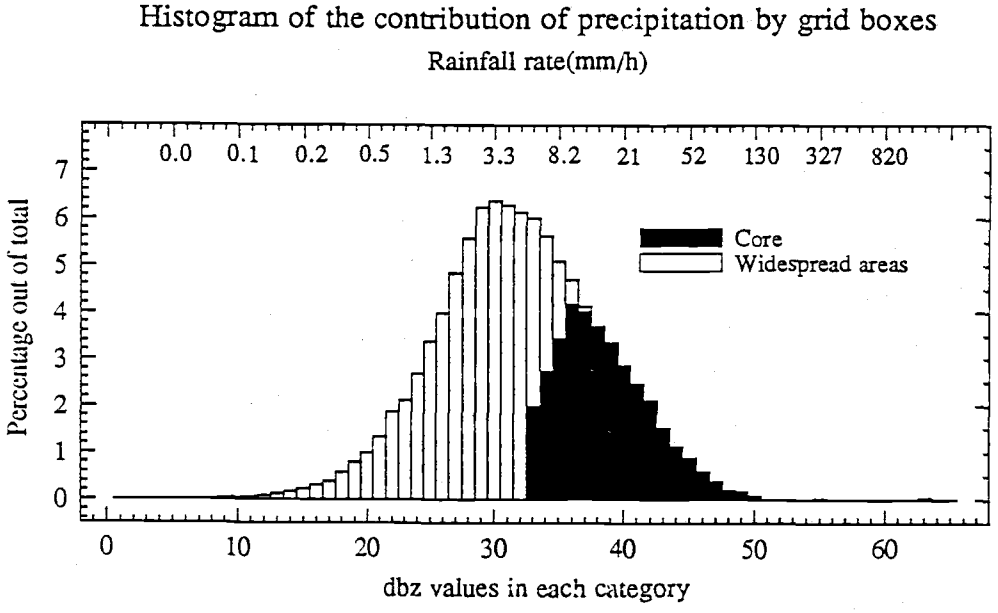

Fig. (2.2.2b) Frequency distribution by the amount of precipitation in each interval

This cut-off value is also supported by the observational study of Crane (1990) who calculated a 12km scale length for adjacent cores over western Kansas in the High Plain Experiment. Therefore a 24km cutoff is large enough to accommodate the cores that are clustered. Figure (2.2.3) illustrates and clarifies the inter-relationships among different entities such as *groups* which are isolated regions of precipitation, *cores* which are found embedded within groups and has associated widespread areas of precipitation, and *clusters* which are constituted by a number of cores close to each other.

Once clusters have been isolated the next step is the computation of the spatial location, area coverage, shape and orientation of each isolated cluster. The spatial location is used to obtain representative vertical profiles of the large-scale horizontal wind and other environmental parameters for each cluster. The area coverage and shape of the cluster are used as parameters for the statistical analysis.

To evaluate the above mentioned simple measures a rectangle was fitted to enclose the cluster, with the major axis being a least-squares fit to the centroids of the cores. This method was simple and straight-forward to interpret and compares favorably with other statistical methods of characterizing size, shape and location. A cluster axis vector was assigned to each cluster with the direction given by the major axis of the box with magnitude as defined in the Appendix A.

In a large number of cases the major axis of the fitted rectangle was close to the axis of the cluster that would have been assigned by a human researcher. In the case of very small clusters the method gives a geometric signature. This is due to the fact that a rectangle is only able to take very specific finite orientations when it is fitted around these small-scale clusters.

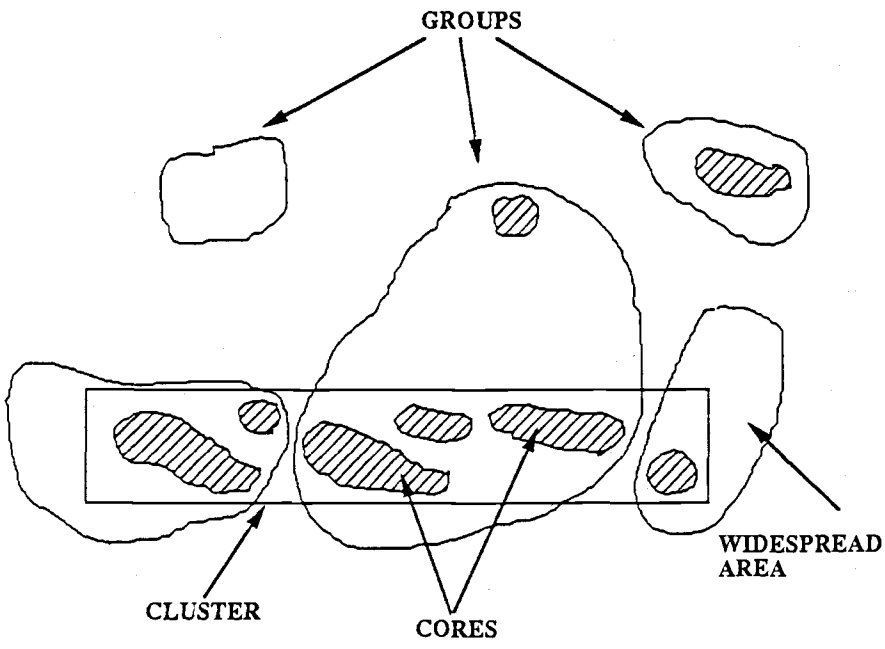

Fig. (2.2.3) Illustration of clusters, cores, groups and widespread areas

Another obvious limitation is in the case where the cluster has a dendritic structure. There is also a directional ambiguity of 180° to the cluster axis vector as described later in Chapter 4.

A simple cluster linearity measure was defined by taking the ratio of the lengths of the sides of the box as given in Appendix A. The area of the box was computed for the clusters to represent the area of influence of the cluster. The centroid of the rectangular box was taken as the cluster center for simplicity and the wind profile at this center was found using the upper-air data. This was used to compute vertical wind shear and other environmental quantities which are used for statistical analysis as explained later in Chapter 4.

The performance of the automated method is checked in Chapter 3 by comparison with other more limited statistical studies by GATE researchers where clusters were identified manually. It is seen that the automated method, though not perfect, performed satisfactorily. To gain insight into the organization of the convective clusters, time series were computed and the results were analysed. The relationship of clusters to large-scale flows were studied and are described in Chapter 4.

3.0 ANALYSIS OF BASIC STATISTICS OF CLUSTERS

In this chapter the precipitation cores identified from the automated method are analysed to identify their basic statistical characteristics. The relationship of the clusters to the total rainfall and vertical motion are studied and compared with the results of previous investigations. From this it is hoped to obtain some validation of the automated methods and to gain further knowledge about clusters.

3.1 Characteristics of widespread areas of precipitation and mesoscale organization of precipitation cores (clusters).

To assess the success of the automated method in picking out the convective cells and associated phenomena we look at statistics such as frequency of occurrence of D, C and B/C scale echo groups which are associated with isolated areas of convective activity as described earlier. See Fig. (3.1.1) for the size categories for each scale. These statistics are compared with similar results obtained by other researchers. All the results are presented for 17 days during the GATE Phase 3 period.

Figure (3.1.1) shows that the statistics of echo groups which are isolated patches of precipitation, are similar to the observed results of Houze and Cheng (1977; see Fig. (3.1.2)) although our results indicate a smaller number of D-scale groups relative to C-scale groups. Houze and Cheng's study was performed on the data from Oceanographer which was closer to the equator and was in the middle of the ITCZ with its low-level southwesterly flow. The Oceanographer was positioned in an area of high convective activity; the Gilliss was positioned in the tradewind flow which produces a different convective regime. It should also be mentioned that in the Houze and

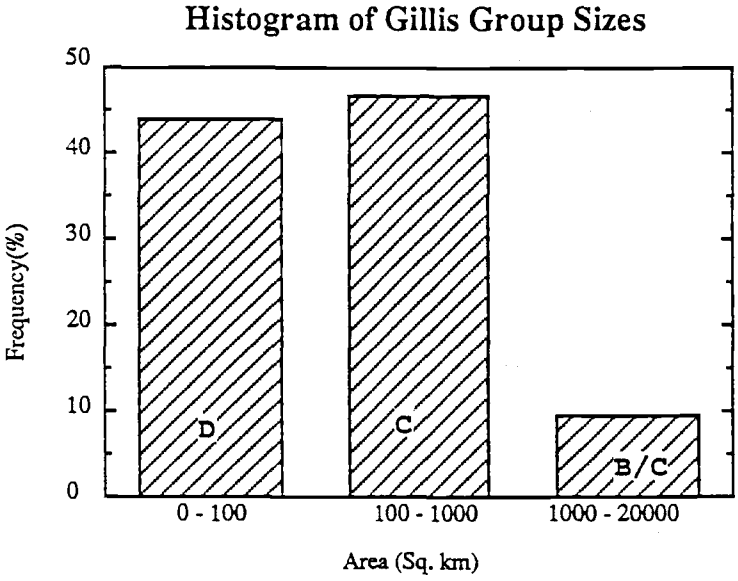

Fig. (3.1.1) Frequency distribution of echo groups from Gilliss

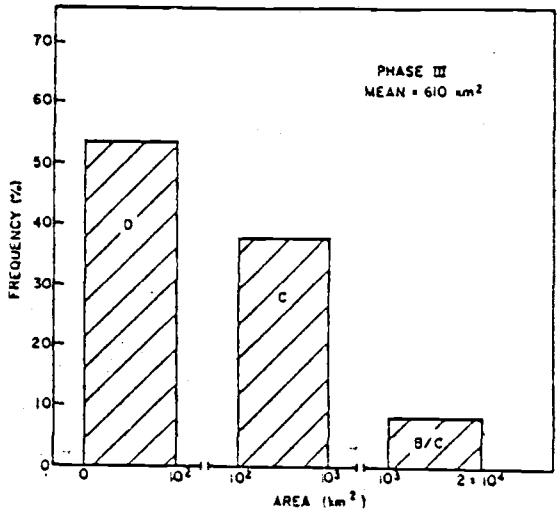

Fig. (3.1.2) Frequency distribution of echo groups from Houze and Cheng's study

Cheng (1977) study, their manual analysis of echo features was done for the data from the early morning at 1200GMT.

The early morning minimum in convective activity may explain the reason for their studies to indicate a higher number of smaller echoes. This kind of a variability is supported by the diurnal nature of the convective systems, as was observed by Tollerud and Esbensen (1985) in their study of the life cycles of nonsquall mesoscale convective systems. They also found that mature stage typically occurred during middle to late afternoon.

The frequency distribution of the nearest neighbor distance between the centroids of the cores is given in Fig. (3.1.3). From this it is apparent that there is a dominant scale length of around 10km. This length scale is close to that observed by Crane (1990) as explained in Chapter 1. Note that the cut-off of 24km for separating clusters is well beyond the median separation of cores and that the distance between clusters was measured not between centroids in the single-linkage cluster analysis, but was between the two points in the clusters that were closest to each other. It could also be argued that this 10km scale length points to a particular type of clustering phenomena among cores. This kind of clustering is consistent with the work done by Ramirez and Bras (1990) who through statistical and observational studies concluded that the spatial distribution of cumulus clouds is regular as opposed to random.

In Fig. (3.1.4) it is observed that the widespread area precipitation lags behind core precipitation as found by Leary (1984) and others. This time-lag of the widespread precipitation is believed to be associated with the development of the mesoscale anvil clouds which persists long after the peak convective activity has ebbed. The decaying system maintains a

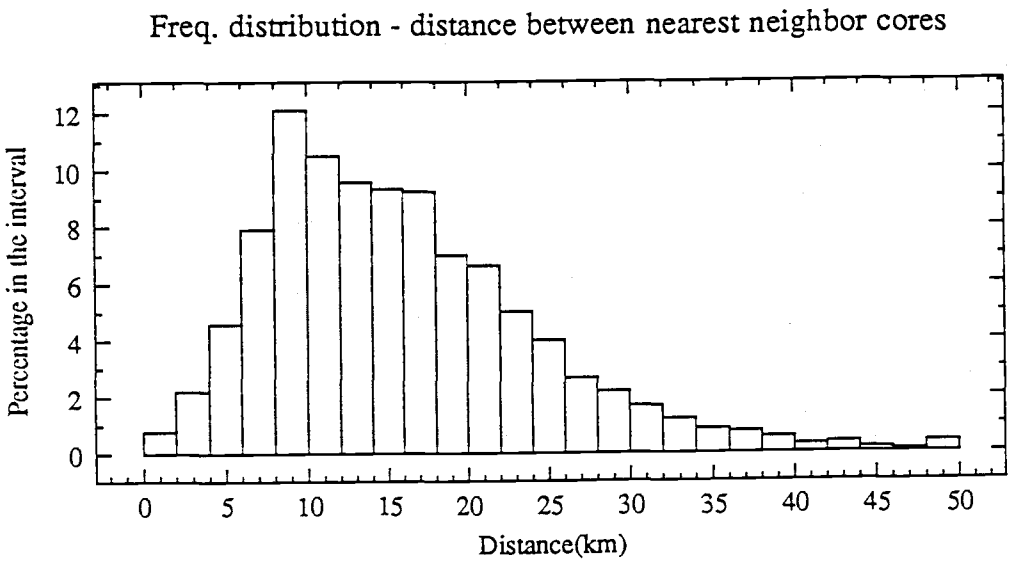

Fig. (3.1.3) Nearest neighbor distance of cores

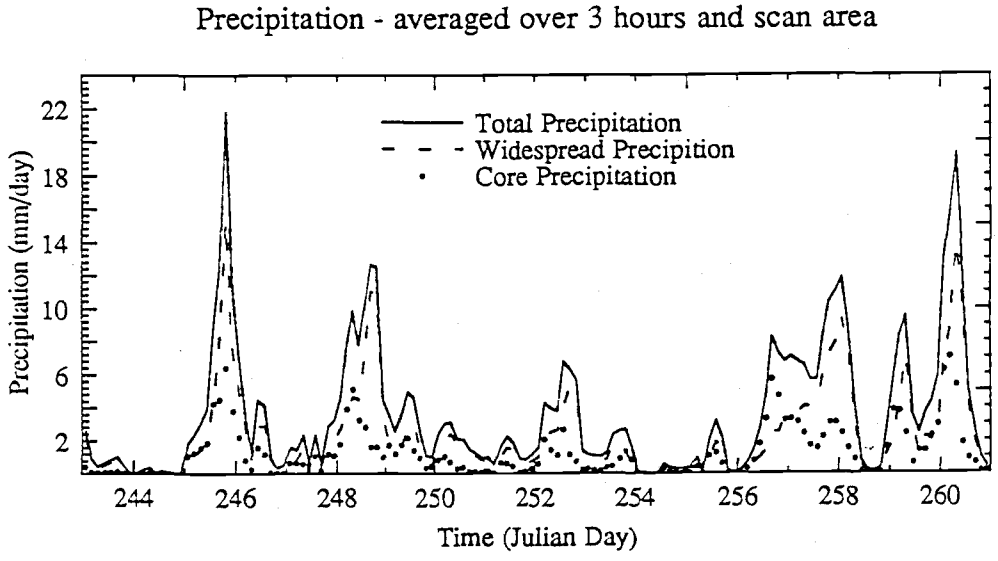

Fig. (3.1.4) Time series - Total, core and widespread precipitation

widespread area of light precipitation.

By looking at the Fig. (3.1.5) we see that the ratio of widespread precipitation to the total precipitation fluctuates between close to 100% to 35% with an average of 64%. Leary (1984) found a 30% coverage ratio for the widespread precipitation for the September 5th GATE cloud systems covered by the four ships. In the Leary (1984) case study, classification of reflectivity was performed manually, and this day was specifically selected to study the double cloud cluster that passed through the GATE region. Looking at Day 249 in Fig. (3.1.5) which correspond to this day we see a percentage in the 50% range. Cheng and Houze (1979) performed a similar study for the Oceonographer data, and found a figure of 50% for Phase 1, 40% for Phase 2, 35% for Phase 3 of GATE. But in their study they considered only the 1200GMT scan data and they acknowledged the importance of the diurnal cycle on the result. They also speculated on the probability of having an error of 10 to 15% due to this and many other reasons. Similar study was done by Houze (1977) for 4-5 September over GATE and he came with a figure of 40% for widespread stratiform rain. In other studies where individual squall-line systems were considered, Gamache and Houze (1984) found that 49% of the rain was stratiform for 12 September case while Houze and Rappaport (1984) found that 42% was stratiform for 28 June case. Similarly Zipser et al. (1981) did a detailed case study of mesoscale convective bands over the GATE region on 14 September and found that 50-55% of the rainfall was from stratiform precipitation. Considering all the studies done with many restrictions such as specific case studies, time periods etc., it can be safely argued that our results are within reasonable limits when considered that it was performed over the whole period of Phase 3 on Gilliss data and

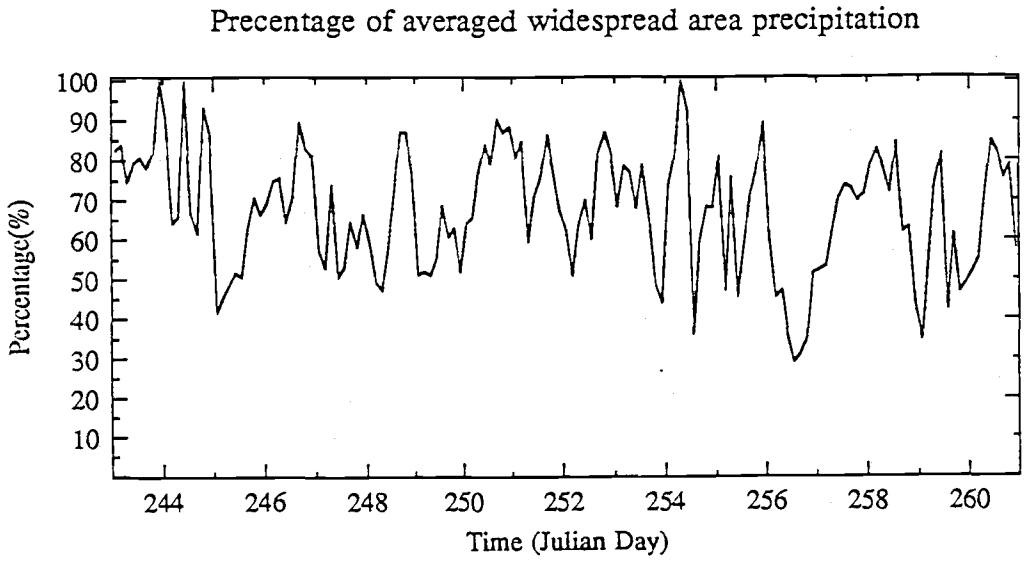

Fig. (3.1.5) Time series - Percentage of the averaged widespread area precipitation

was done by automated methods as opposed to manual methods of the other studies. It should also be pointed out that in our study, all light precipitation was included in the widespread precipitation category thereby tending to increase slightly its share of the total rainfall.

3.2 Cluster area as a scaling factor in precipitation

One of the very important results from this work is that the area of the large cloud clusters can be used as a scaling factor to determine the total precipitation of the organized mesoscale convection and also as a contributing measure to gauge the total precipitation in mesoscale systems. This conclusion is based upon observing the time series of factors such as total precipitation, area covered by clusters and their precipitation as described below. These relationships are explained by the fact that large precipitation events are characterized by strongly active convective cells which are shown to be well organized in space. These cells are embedded in stratiform areas whose extent could be argued to be a function of the strength of the convective cells.

Figure (3.2.1) gives the areas of large clusters (C and above) and D-scale clusters, and the Fig. (3.2.2) gives similar time series with a small modification of adding the area of single cores to the clusters. All of the above mentioned time series were averaged over the scan area of the radar and over a 3-hour interval to smooth the data and to give a common base for comparison. From these two figures it can be inferred that single cores and small-scale clusters make very little contribution to the total cluster area especially in the cases where major events are taking place.

There is a very high correlation between widespread precipitation rate

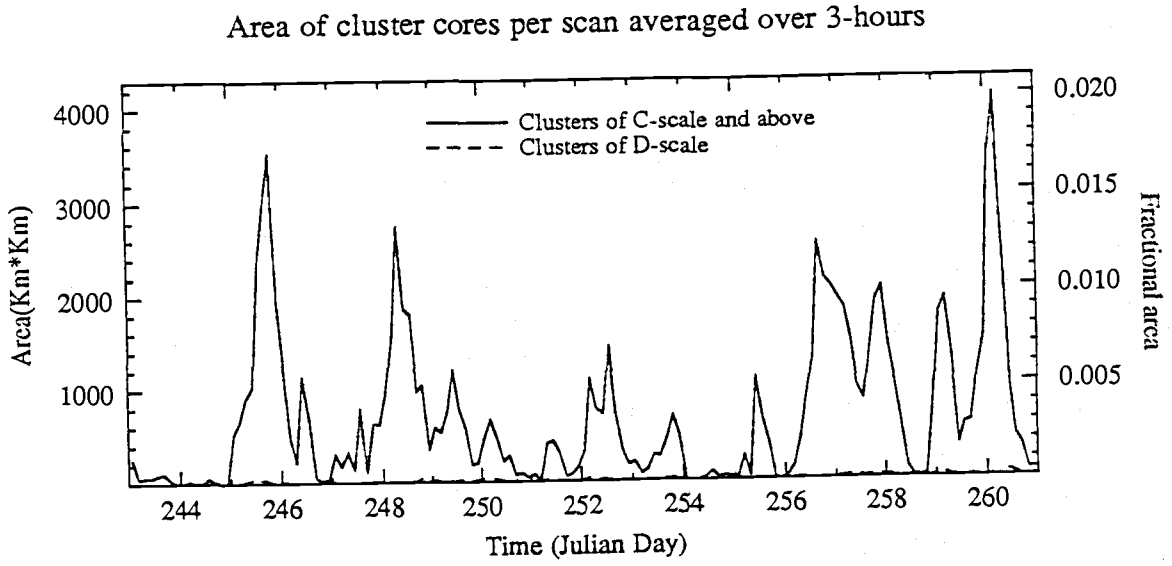

Fig. (3.2.1) Time series - Area of clusters - D, C and above scale

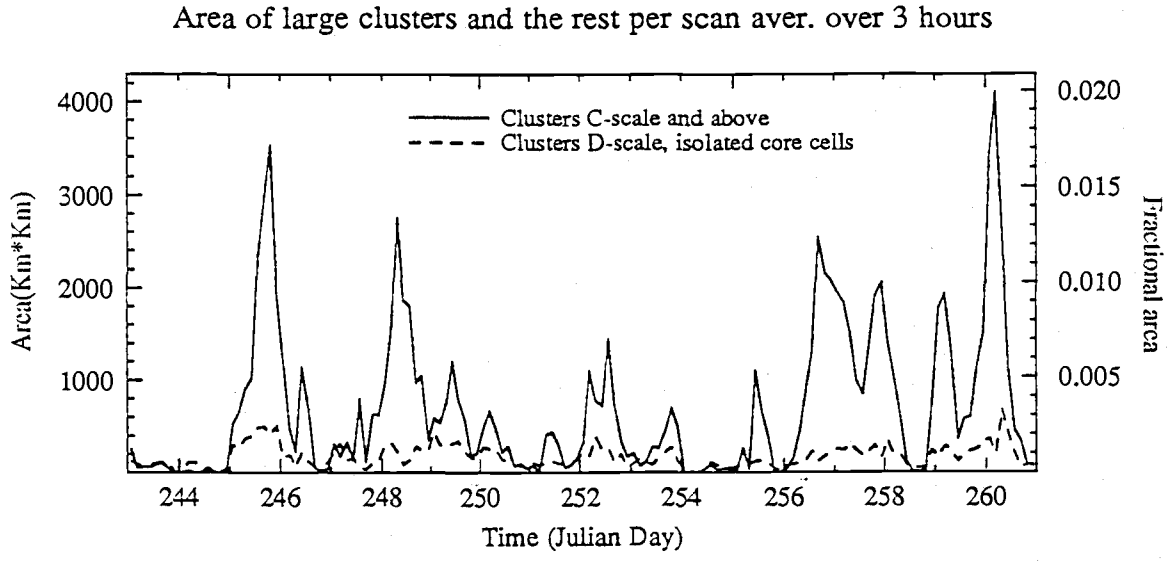

Fig. (3.2.2) Time series - Area of large-scale clusters, small-scale clusters and isolated cores

and the extent of coverage by the widespread areas. This can be easily seen in the time series shown in Fig. (3.2.3a) and also by the scatter plot given in Fig. (3.2.3b). The statistical computations given below and similar computations done later in this chapter were executed using International Mathematical Sciences Library routines and the algorithms for these particular routines are based on Neter et al (1985). The corresponding data has a linear regression coefficient of 0.96 and with a second order curve fit the correlation index improved to 0.97. Using the t-test and the hypothesis that the coefficient of the second order term is equal to zero with a significance level of 0.05, it was concluded that the coefficient of the second order term was not equal to zero. The equation for this second order fit is : Average widespread area precipitation (mm/day) = 0.013 + 23.69 * (Fractional area) + 104.96 * (Fractional area)^2. The fractional area is the fraction of the scan area covered by the widespread area precipitation. For the coefficients, the Boferroni joint confidence intervals (see Neter et al, 1985) at 0.90 significance level are : 0.013$\pm$0.249, 23.69$\pm$6.44 and 104.96$\pm$29.39.

The reason for the second-order fit could be that widespread areas are made-up of light stratiform precipitation areas of relatively even strength, but with larger stratiform areas it may be speculated that they contain relatively protected and active mesoscale regions with higher precipitation rate than smaller systems.

The clusters of precipitation cores and their areas also show a somewhat similar relationship as indicated by their time series given in Fig. (3.2.4a) and the scatter plot between them as illustrated in Fig. (3.2.4b). The relationship between them appears to be strongly linear with a linear regression coefficient of 0.99. Using the t-test as explained earlier the coefficient of the

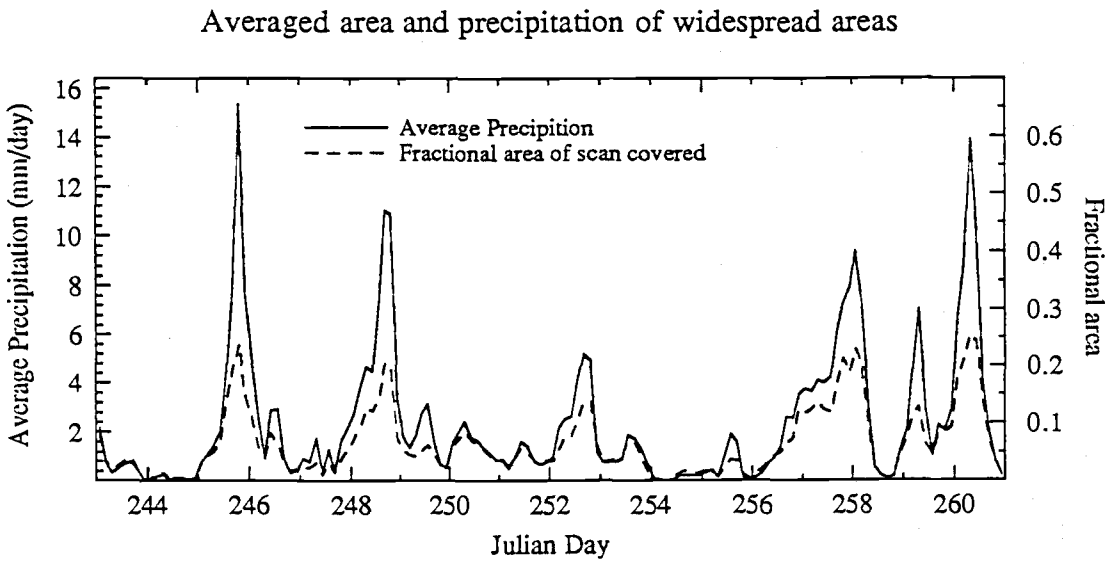

Fig. (3.2.3a) Time series - Area and precipitation of widespread areas

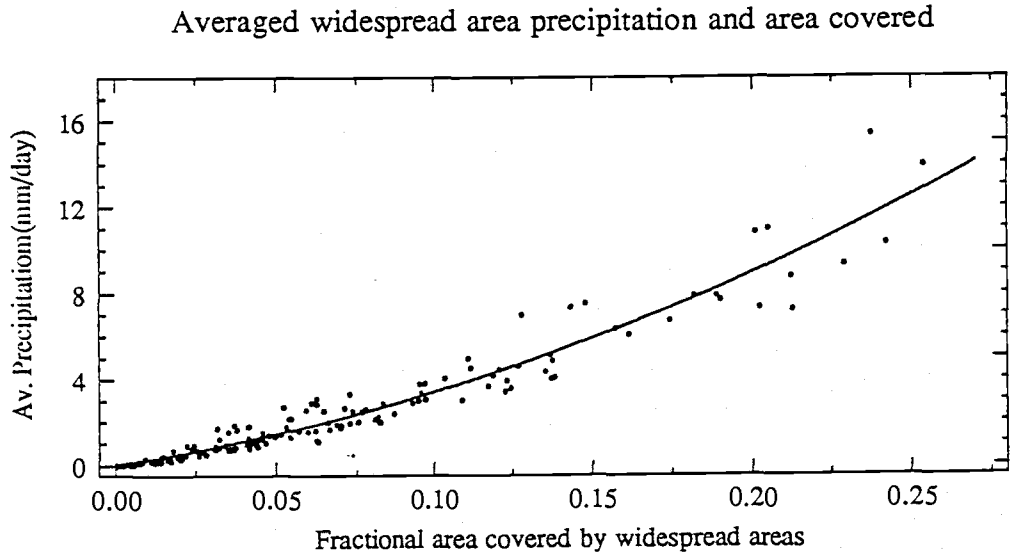

Fig. (3.2.3b) Scatter plot and second order fit for Fig. (3.2.3a)

1st order term was found to be significant. The linear equation for this relationship is : Average cluster precipitation (mm/day) = -0.08038 + 0.00169 * (Area of clusters). Here the area is measured in square km. The confidence intervals for these coefficients are : -0.08038±0.04949 and 0.00169±0.000039. The area of the clusters in a scan is found by computing the core area of the clusters of large-scale.

The reason for this linearity could be explained if the convective cells which constitute the clusters have relatively similar strength. Thus the larger the area covered by clusters, the larger the number of strong convective cells, while the precipitation amount per unit area remains more or less constant. This is apparent from Fig. (3.2.8) and (3.2.4a). They show that during major events, the area covered and the number of cores are strongly correlated. With this observation of the close correlation between area of large-scale clusters and time series of cluster rainfall, with peaks characterizing major precipitation events, it could be argued that the cluster-core area can be used to parameterize the convective precipitation in mesoscale convective systems.

The relation between the total precipitation and fractional area covered by the widespread areas of precipitation was investigated. The Fig. (3.2.5a) gives the time series between these two quantities and Fig. (3.2.5b) gives the polynomial fit between them. The time series shows a good correlation with a linear correlation index of 0.936 and a slight improvement to 0.939 for the second order fit. The coefficient of the 2nd order term was marginally significant. The linear equation is given by : Average total rainfall rate (mm/day) = -0.526+ 63.233 * (Fractional area of widespread areas). Here the fractional area is the fraction cover by the widespread area of precipitation within the scan area. The confidence intervals for the coefficients

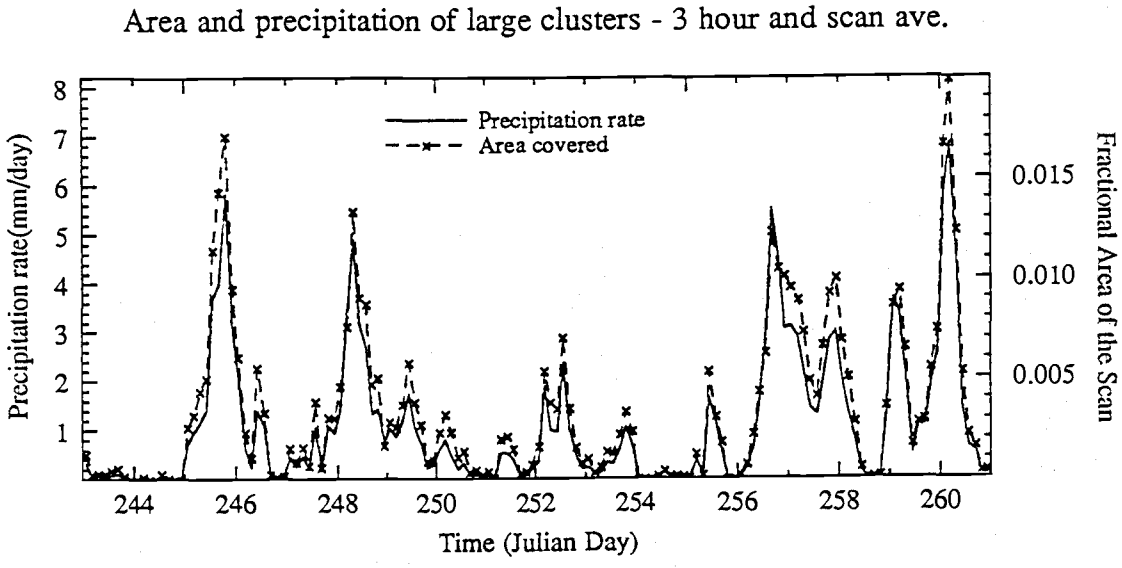

Fig. (3.2.4a) Time series - Area and precipitation of large-scale clusters

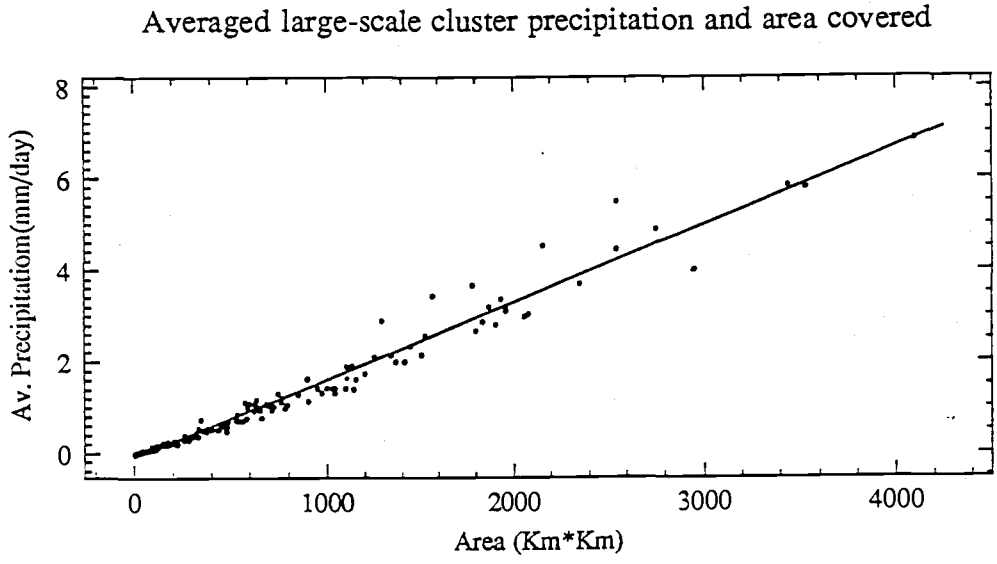

Fig. (3.2.4b) Scatter plot and linear regression fit for Fig. (3.2.4a)

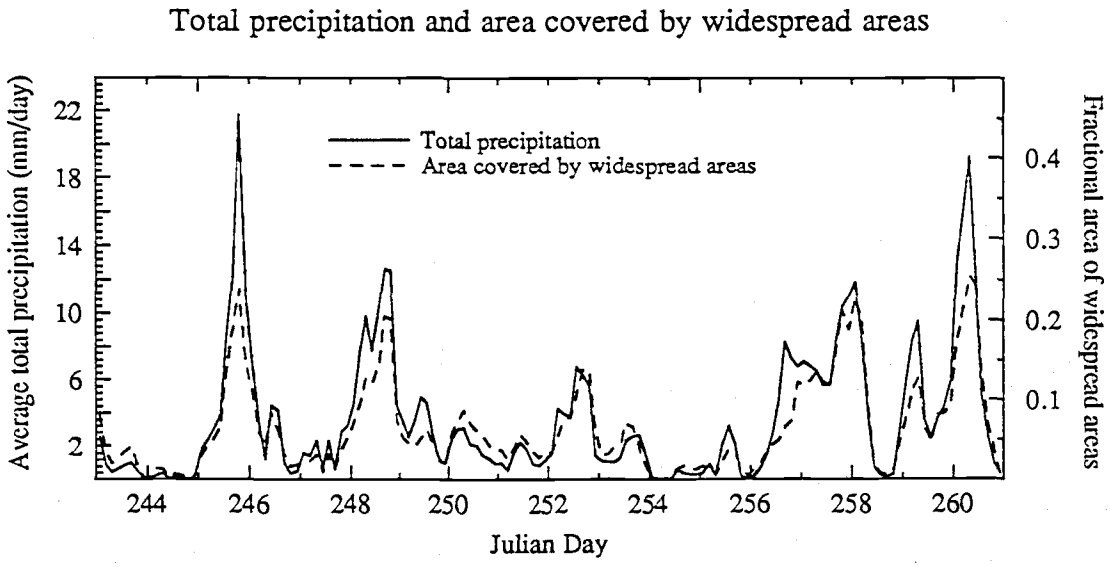

Fig. (3.2.5a) Time series - Total precipitation and area of widespread areas

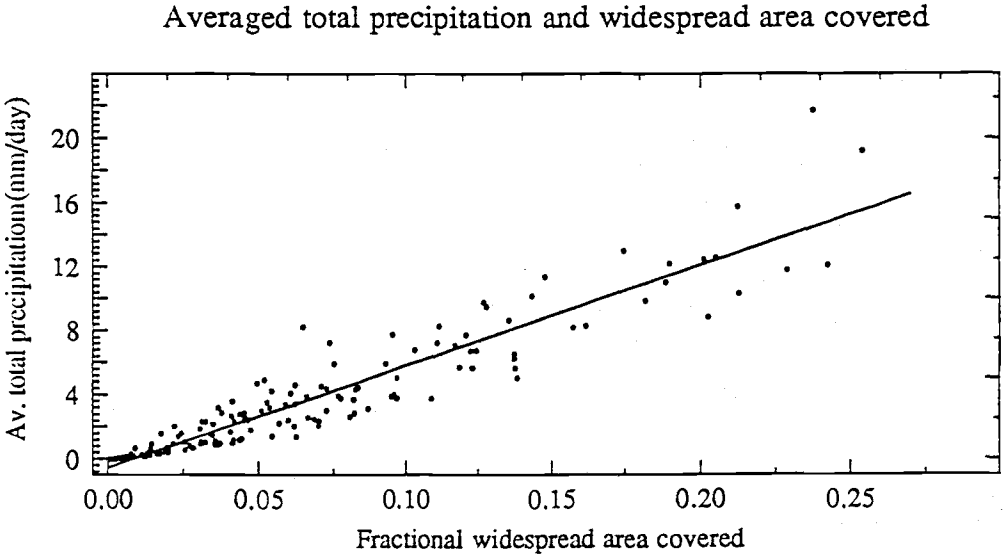

Fig. (3.2.5b) Scatter plot and linear regression fit for Fig. (3.2.5a)

are : -0.526±0.339 and 63.233± 3.808. But it should be mentioned that the variance explained by the fit was reduced due to the scatter in the data. It is apparent that if the total cloud cover is known the total precipitation could be estimated to a certain accuracy. But if the widespread areas and clusters could be differentiated then as indicated by earlier figures the estimate could be done with an extremely good accuracy.

Another interesting relationship is the somewhat close correlation of the time series of cluster area in Fig. (3.2.1) and the total precipitation in Fig. (3.1.4). To investigate this further a scatter plot of total precipitation averaged by scan area and the fractional area covered by large-scale clusters was done and is given in Fig. (3.2.6). This has a linear correlation coefficient of 0.89 and using linear regression analysis the following equation was deduced : Averaged total precipitation rate (mm/day) = 0.645 + 914.347 * (Fractional area covered by clusters). The confidence intervals for the coefficients are : 0.645± 0.392 and 914.347± 75.519. Therefore it is apparent that this relationship has a very big error margin compared to the earlier relationship where the area of the widespread areas is used as the independent variable for predicting the total precipitation. It is also apparent from the large scatter in the plot.

Figure (3.2.7) and Fig. (3.2.8) show the time series of number of cores in clusters of large-scale and of all scales, respectively. When these time series are compared with the time series of total precipitation given in Fig. (3.1.4) it reinforce the already known fact, that major precipitation events are characterized by a large number of convective cells and major events are well represented by considering only the large-scale clusters (Houze and Cheng, 1977). The Fig. (3.2.9) gives the number of clusters as a time series. It is evident from these figures that the large number of cores in major

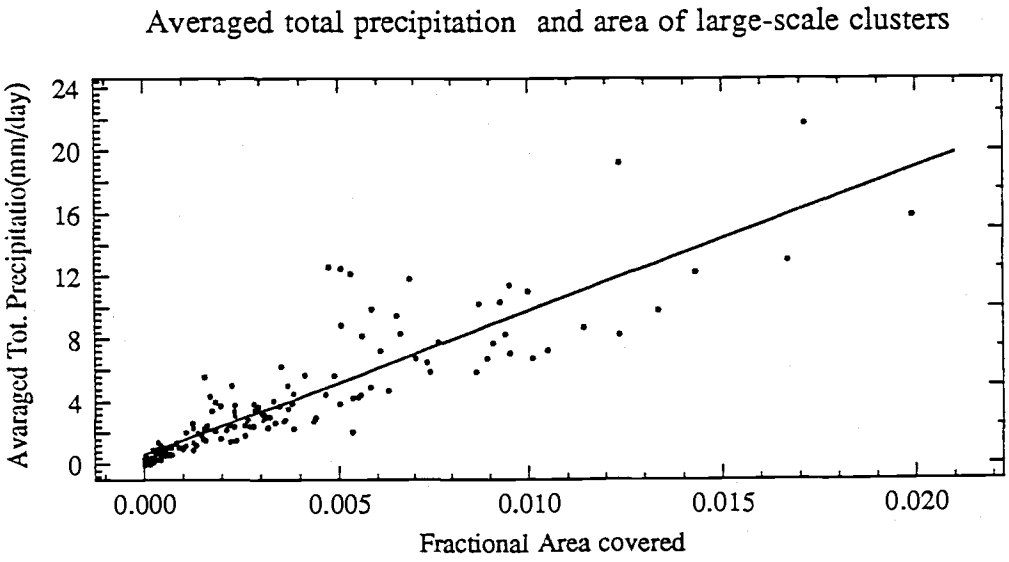

Fig. (3.2.6) Scatter plot and linear regression fit between total precipitation and cluster area

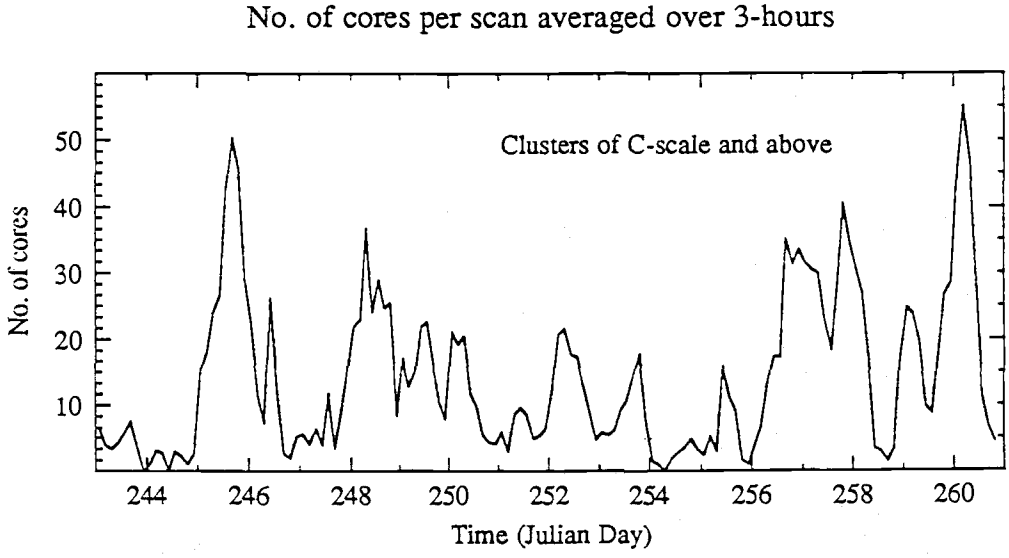

Fig. (3.2.7) Time series - No. of cores in large-scale clusters in a scan

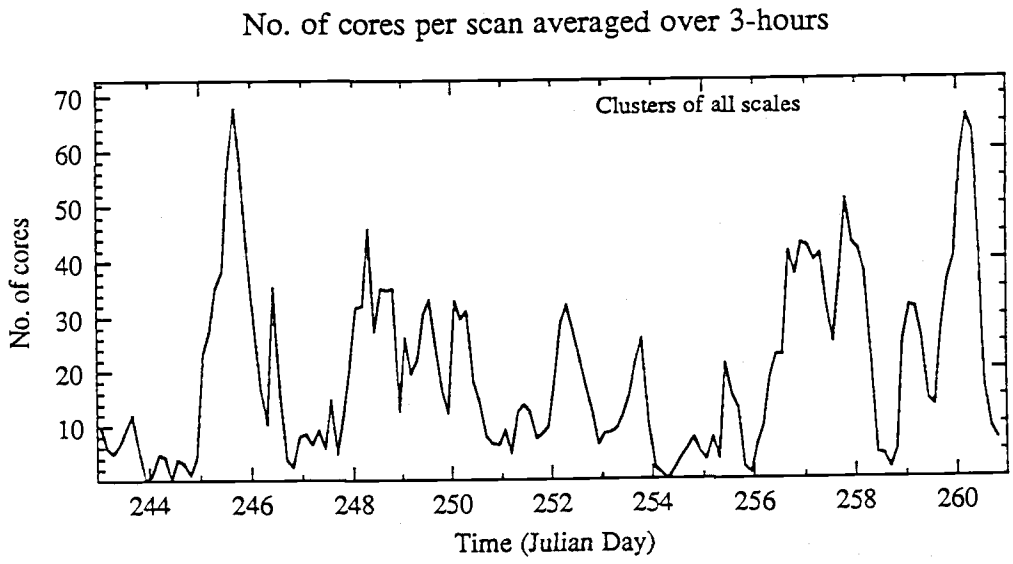

Fig. (3.2.8) Time series - No. of cores in clusters of all scales in a scan

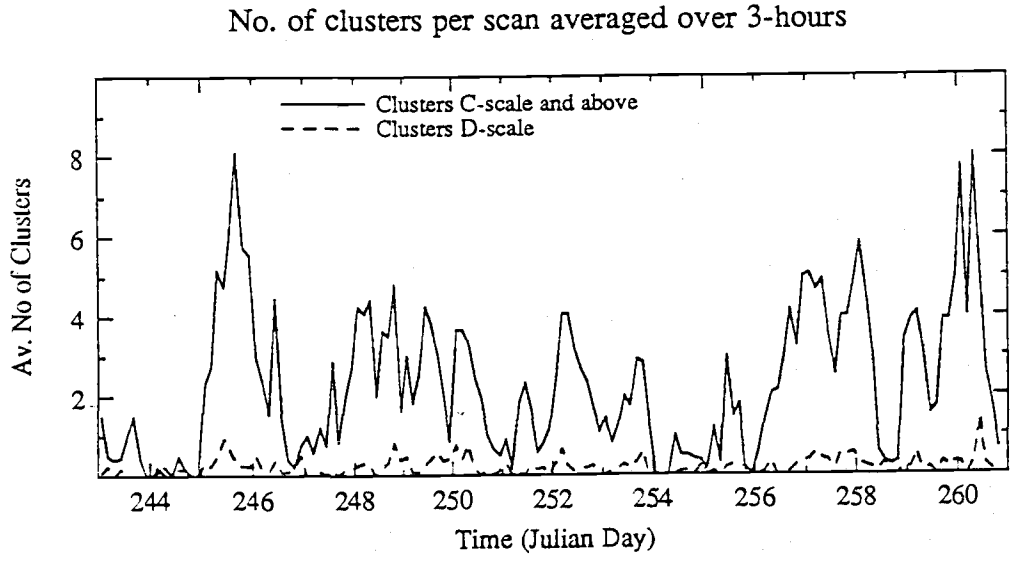

Fig. (3.2.9) Time series - No. of clusters in a scan

precipitation events tend to organize into large number of clusters. Thereby indicating a clustering phenomena among cores. It is also seen that the number of clusters of small-scale in comparison with the large-scale clusters is very small. The reason for this could be attributed to the rectangular area method by which the cluster scale size was compute. The area for the D-scale, when compared with the grid area was small thus creating a situation where the possibility of being a D-scale cluster was small.

3.3 Relationship to large-scale vertical motion

The large-scale vertical motion was computed by averaging the vertical velocity spatially over area of the radar scan of interest at 3-hour intervals. The vertical motion field was archived at 3-hour intervals and represents meso-α scale motions. Statistics of the precipitation field were averaged for radar scans falling within a 3-hour window centered on the archived time for the vertical motion.

Looking at the average large-scale vertical motion and precipitation in Fig. (3.3.1), it can be concluded that the large-scale vertical motion is correlated well with the widespread precipitation at levels around 400mb, while for cores the correlation is relatively uniform with height. The correlations are illustrated by the time series of precipitation and vertical motion at 400mb in Fig. (3.3.2). The time-height section for vertical motion is given in Fig. (3.3.3) to give an idea of the motion at different levels. The confidence intervals for the peak values of correlation coefficient found in the plots were computed using Fisher's z - transforms. Using a confidence level of 95%, it was found that for a correlation of -0.63 the interval was

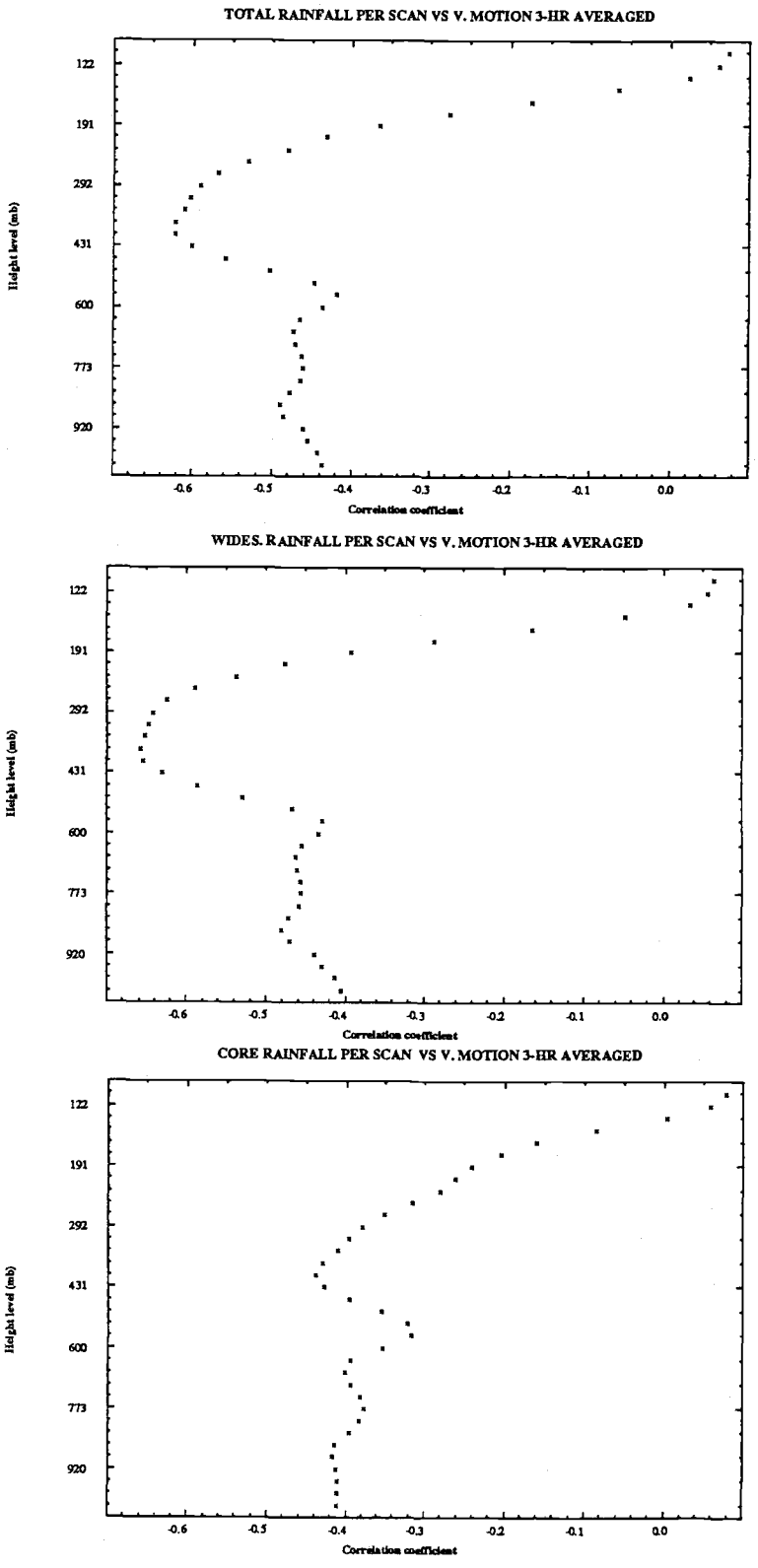

Fig. (3.3.1) Correlation of vertical motion with core, widespread and total precipitation

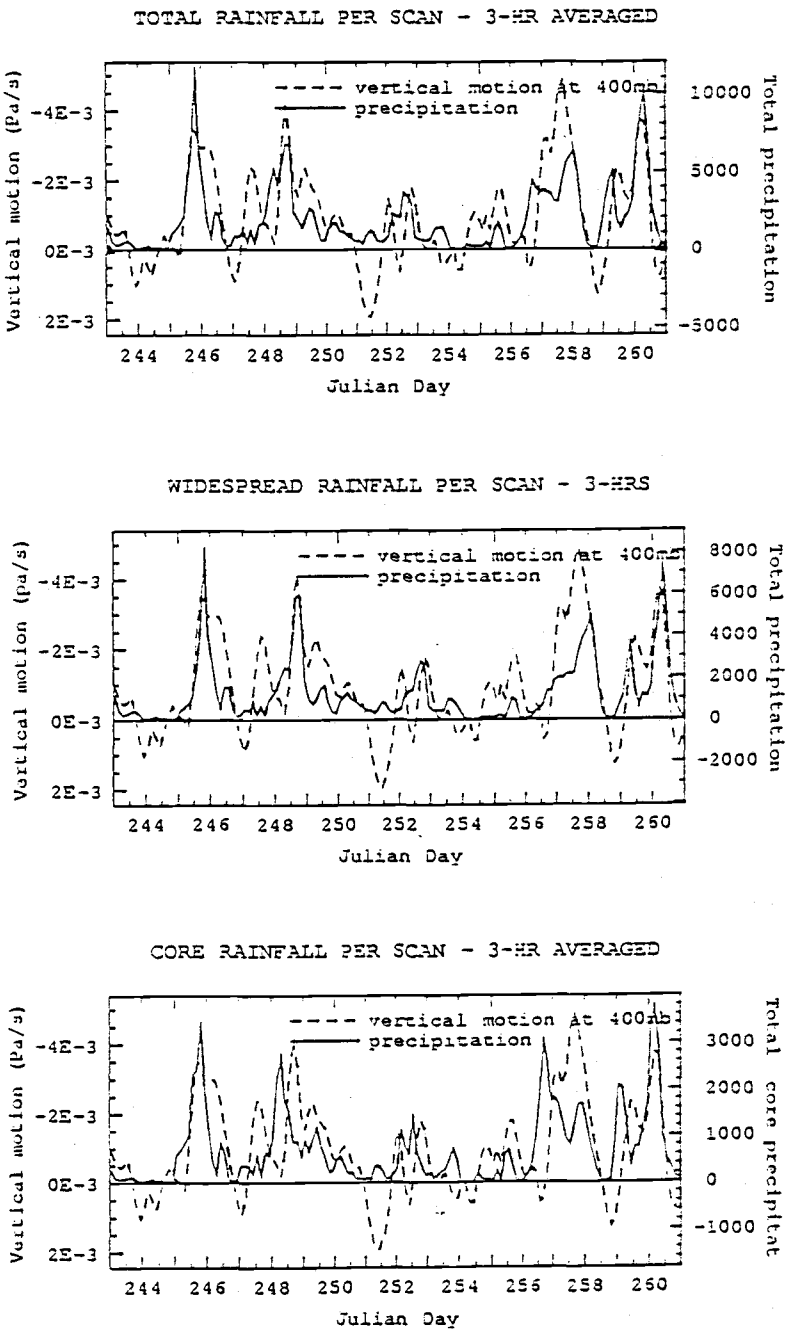

Fig. (3.3.2) Time series - Vertical motion at 400mb and precipitation of cores, widespread and total

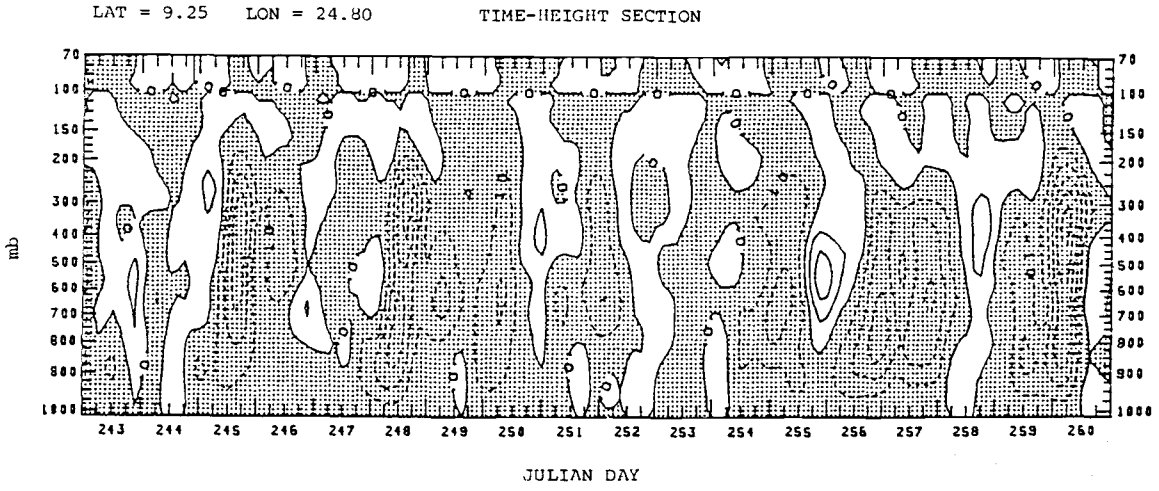

Fig. (3.3.3) Time height section of vertical motion.
The motion meso-α-scale $\omega(=dp/dt)$.
Contour intervals ($\times 10^{-2}$ Pa.s^{-1}) at
-50, -40, -30, -20, -10, 0, 10, 20 .

from -0.71 to -0.53 and that for -0.4 it was from -0.52 to -0.27. Therefore it is seen that the value of -0.63 for the upper-level correlation of vertical motion with widespread and also total precipitation is very significant.

The correlation of widespread precipitation with upper-level vertical motion is expected on the basis of previous case studies and composite results (Houze and Betts, 1981). In general mesoscale uplifting at upper levels is required in the stratiform region to maintain the light precipitation. In our study we found that the level around 400mb had the highest correlation as seen from the Fig. (3.3.1).

For the case of convective cores it is apparent that there is no preferred level. If the vertical motion was resolved on the convective scale and the vertical motion at the core centers were considered then a lower-level maximum in the correlation might be expected. This is because large updrafts in convective scale at lower levels will give rise to larger convective towers in the mature stage of their development as dictated by the dynamics with a resultant higher precipitation contribution (Rogers 1979). But in this study we considered the mesoscale vertical motion and not the convective scale. This vertical motion was the average motion over the scan area and it was averaged over a 3 hour interval to remove lower-scale motions. Therefore this may explain the reason for not showing any preferred level of correlation for cores. In the case of total precipitation it is seen that it has preferred correlation at a level that is almost the same as that of widespread precipitation. This is easily explained when one considers the fact that a large percentage of the total precipitation is constituted by the widespread area precipitation.

4.0 ANALYSIS OF RELATIONSHIPS BETWEEN CLUSTERS AND LARGE-SCALE HORIZONTAL WIND FIELD

To explore the relationship between clusters of precipitation cores and large-scale horizontal wind field, several techniques were used including a tensor correlation between wind shear and cluster linearity vector, and a chi-square technique to distinguish the distribution between the angular separation of the wind shear and the cluster linearity vector from a uniform distribution. The first step was to determine the layer over which the wind shear was most strongly correlated with cluster orientation. The statistics of the angular separation between the cluster orientation and wind-shear direction were then computed and summarized.

In the evaluation of the relationship between wind shear and the orientation of cloud bands, a way must be found to statistically summarize the large amount of data. The analysed wind velocity is given at 41 height levels, and there are numerous parameters that describe cloud organization. In this analysis we use a linearity vector to denote the orientation of the cluster, with a direction which coincides with the least square regression line fitted to the cluster core centroids as explained in Chapter 2 and a magnitude as given in the Appendix A. A major difficulty in the analysis is the problem of directional ambiguity; cluster direction can be assigned in two directions that are 180° apart as illustrated by Fig. (4.0.1).

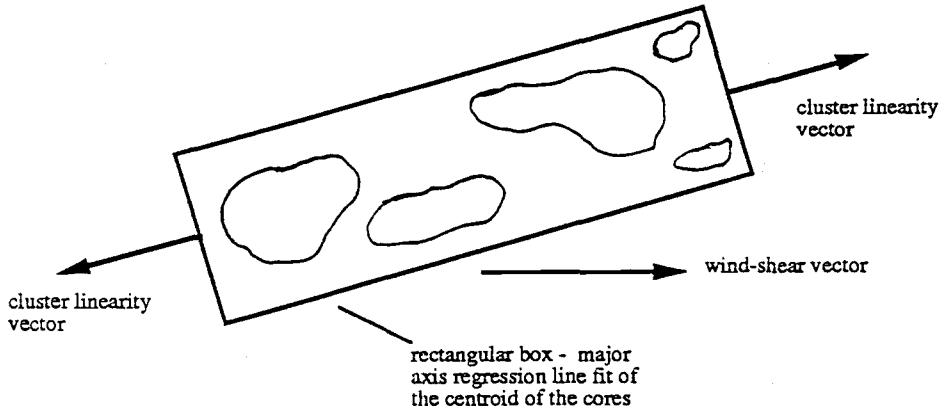

Fig. (4.0.1) Illustration of cluster linearity vector

4.1 Polar representation of tensor cross-spectra of linearity and wind shear

4.1.1 Method

The tensor correlation method proposed by Ooyama (1985) was used in this analysis. Since the second statistical moments of vector variables are tensors, the properties of the tensors can be used to simplify the analysis. In Ooyama's method the tensor invariant properties of the wind covariance are preserved after normalization by the variance tensor. A more detailed description of the method is given in the Appendix B.

The shear of the wind between two height levels was computed at the center of each cluster; linearity vectors were computed for the cluster as described in the Chapter 2. To resolve the 180° directional ambiguity in the linearity vector, the direction was chosen in such a way that an acute angle was formed between the wind-shear vector and the linearity vector.

As the relationship of interest was between wind shear and linearity vectors and not between their variations from the means, both the wind shear and linearity vectors were provided with associate vectors, equal in magnitude but 180° from the original vectors. This made the mean of the each vector zero but it kept their directional orientation from each other intact. Even though this modification brought about the desired property, it created additional problems which were partly due to the fact that the linearity vector was always within ±90° of the wind-shear vector, and are described later. Since we are interested in only the directional relationship between the wind-shear vector and the linearity vector, clusters of linearity greater than 0.1 were considered and the magnitude was assigned the value

of unity.

It should be stated that a set of random vectors of similar characteristics will also have a large correlation in the horizontal direction under the above mentioned conditions. Another problem that should be guarded against is, that at edges of the angular domain of the vectors, the separation angle can fluctuate from negative to positive for very slight changes in the orientation of the cloud bands with respect to the wind shear. All these factors necessitated the sensitivity analysis of the correlation vector. For this the wind-shear vector was rotated by an angle of 30° counter-clockwise (CCW) and the correlation was computed. The amount of CCW rotation in the correlation vector gives an indication of the sensitivity of alignment between the wind-shear and the linearity vectors.

4.1.2 Results for tensor correlation method

Figure (4.1.1) and Fig. (4.1.2) shows the correlation between the wind shear and the cluster linearity for the scales C and B/C respectively. The D-scale was not considered due to the earlier mentioned problem which is geometric in nature. The computations were separated according to spatial scales to account for any changes in the relationship due to the area of coverage of the cluster. This is justifiable as different scales may have different relationships to large-scale flow as it's influence on their evolution may be of varying levels. In this analysis the counter-clockwise angle of the correlation vector from the positive horizontal axis indicates that the wind-shear vector is ahead of linearity by that particular angle. In the figures the dark arrows give the correlation and arrows with the dashed lines give the correlation where the wind-shear vector has been rotated by 30°CCW.

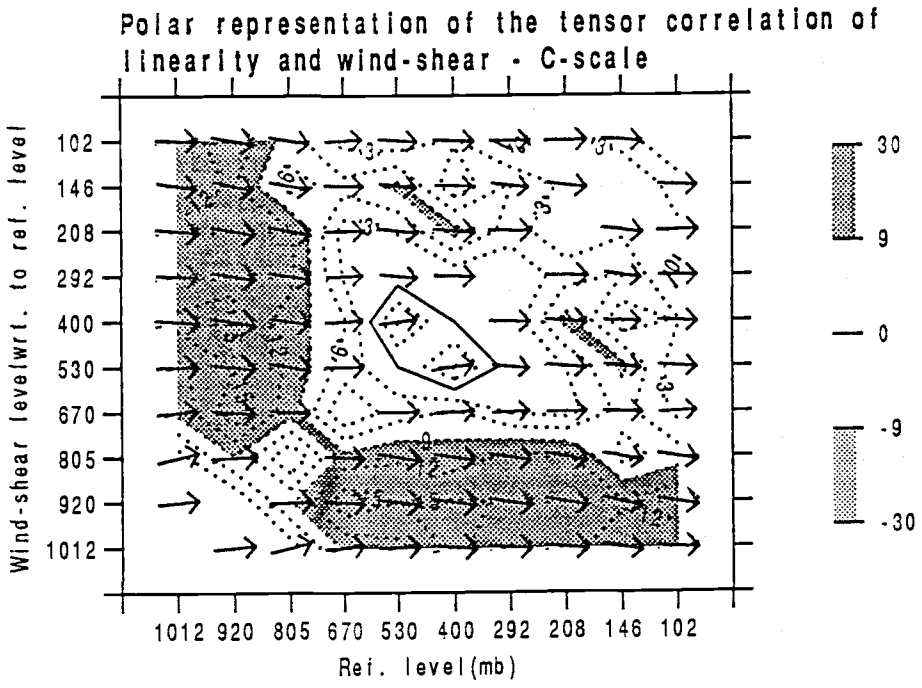

Fig. (4.1.1) Correlation of wind shear and cluster linearity for C-scale clusters. Contours indicate the sensitivity from random distribution. The arrows give the correlation vector.

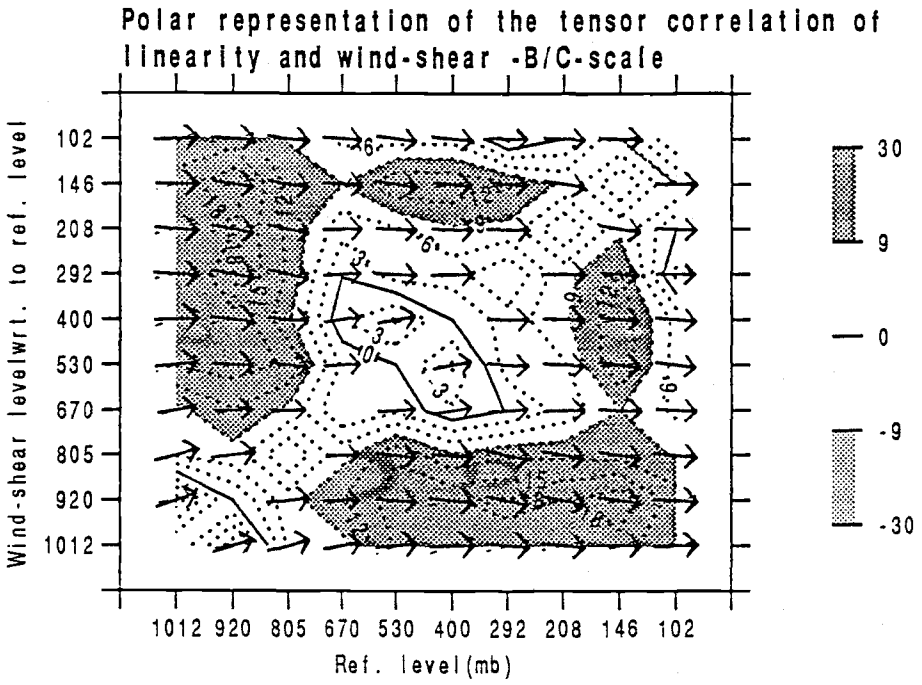

Fig. (4.1.2) Correlation of wind shear and cluster linearity for B/C-scale clusters. Contours indicate the sensitivity from random distribution. The arrows give the correlation vector.

The contours give the angular difference between the rotated case and the non-rotated case with positive values corresponding to the desired rotation. This measures the sensitivity of the alignment of the cluster linearity vector and the wind-shear vector. As explained earlier a correlation vector in the positive horizontal direction may indicates close alignment as the angle that measures whether one entity is statistically ahead of the other is zero.

From the figures it is seen that the sensitivity is highest for the wind shear at levels above 670mb with respect to surface. It is also seen from the contours that the sensitivity increases for the B/C-scale in this region. In this region of high sensitivity it is apparent that for both the scales the correlation vector is close to horizontal in the positive direction. Therefore it could be stated with some reservation, that the alignment of the linearity and wind-shear vectors got better with bigger scales for wind shear computed with respect to sea-surface level. But it should be stated that this method failed to give a very conclusive result. By failing to highlight exclusively or very prominently a specific level where the sensitivity was highest, this method failed in the objective reason it was employed.

From the above reasoning it is apparent that the tensor correlation method did not work in the way it was hoped it would. This is due to the low variability of the wind-shear direction for the most part and also due to the maintenance of an acute angle between the wind shear and linearity vectors. These factors would explain the almost horizontal vectors we seen in these two figures, and also the low sensitivity. Considering all the variabilities present in the linearity vector orientation with the above mention characteristics of the wind shear and the fact that this method gives equal weight to all the data would explain the limitations of this method as applied

to this study. These limitations acted as an impediment for the effectiveness of this method in giving very specific conclusions

4.2 Probability density function representation

4.2.1 Method

This method uses chi-square values of the difference between the probability distribution of the angular separation of the wind shear from cluster linearity and the uniform distribution. The analysis is done for C- and B/C-scale clusters only since discretization errors affect the directions assigned to cluster configurations for D-scale clusters as explained in Chapter 2. Even C-scale distributions show this problem to a certain extent, but are within acceptable limits. The formula for the chi-square calculation is :

$$\chi^2 = \sum_{m=1}^{n} \frac{(f_o^m - f_i^m)^2}{f_i^m}$$

f_i^m - theoretical frequency distribution

f_o^m - observed frequency distribution

n - total no. of frequency intervals

4.2.2 Results of probability density function method

Table 1.0 gives the chi-square values for 10 wind-shear levels with 10 reference levels used in the computation of the wind shear. This symmetric grid shows that for the B/C-scale there are two peaks in the case where the wind shear is computed with respect to surface level - one at 670mb and the other at 208mb. Similarly there are peaks at 208mb and 146mb with reference to 920mb and 530mb respectively.

Table 2.0 shows the results for the probability density function for the

wind shear of 670mb-1012mb layer. Here it is seen that with a higher magnitude cut-off, the local wind shear lies closer to the mean wind-shear direction. Similar relationships are seen for the other layers with the exception that the peaks in the histogram are shifted from the mean wind-shear direction. This is indicated by a shift in the peak away from 0°. This bunching of wind-shear vectors in a preferred direction may explain the reason for the poor performance of the tensor correlation method.

Table 3.0 gives the alignment of the local time-varying wind-shear vector between the levels of 670mb-1012mb, with the linearity vector. Table 4.0 shows similar results with the exception that the linearity is compared with the time-independent mean wind shear. Here, the cases with the specified magnitude cut-off of local wind shear were compared with the mean wind-shear direction. Comparing these two tables it is evident that in the case of local wind shear there is a marked sensitivity with the magnitude of the wind shear, while in the case of mean wind shear the results remain more or less uniform. Comparing with results of other layers (not shown), it was found that this sensitivity was highest for the 670mb-1012mb layer.

For other layers with chi-square maximum, it was found that the local wind shear with respect to mean wind shear was restricted to a narrow band. And in some of the cases the local wind shear had a direction close to that of the mean wind shear between the 670mb-1012mb. Therefore it is obvious that the distribution of angular separation of wind shear with cluster linearity would have high chi-square values at these levels too. As the earlier mentioned layer of 670mb-1012mb with high chi-square had the characteristic of wind shear being bunched together, any layer with similar characteristic would also have a high chi-square value.

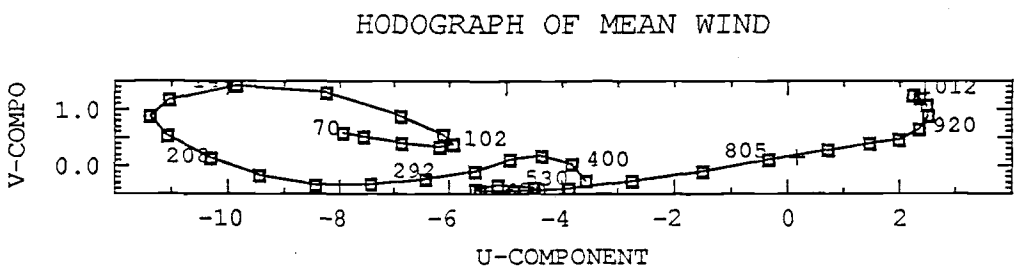

Fig. (4.2.1) Hodograph of mean wind

Only difference may be the shift in the peak of the distribution which would correspond to the mean angle of the bunched vectors. From the hodograph of the mean wind with height given in Fig. (4.2.1), it is apparent that the directions of the mean wind shear at levels of interest differed by 30 degrees or less in most cases. This explains the shift observed in these cases. Finally it should be stated that the horizontal wind profiles used in this study had a direction confined to a very narrow range. This is somewhat apparent from hodograph and Table 2.0. This lack of variability in the local wind shear in many levels gave high chi-square values at these different levels. The local wind shear profiles and the mean wind shear profiles had similar directions, thus making it very hard to come to a definite conclusion on the influence on clusters from wind shear at a particular level.

In the future these methods should be applied to other data sets to explore a wider range of wind shear situations.

Table 1.0 **Chi-square values of separation angle with respect to uniform distribution**

The chi-square values of the distribution of the separation angle of wind-shear with respect to cluster linearity vector, that differed from the uniform distribution are given below. The computations are done for two scales and for 10 wind-shear levels with reference to these 10 levels.

Ref. level(mb)		1012	920	805	670	530	400	292	208	146	102
	level										
Scale	102	16.1	17.0	10.2	2.0	2.8	3.1	2.9	2.9	3.8	0.0
B/C	146	19.1	22.9	8.4	4.4	18.2	17.9	6.2	9.7	0.0	3.8
	208	26.4	24.2	13.8	3.0	3.8	3.9	4.4	0.0	9.7	2.9
	292	25.1	20.2	9.8	2.4	2.0	1.7	0.0	4.4	6.2	2.9
	400	20.8	13.8	4.1	10.9	6.0	0.0	1.7	3.9	17.9	3.1
	530	17.9	17.1	5.4	9.5	0.0	6.0	2.0	3.8	18.2	2.8
	670	20.4	19.4	13.3	0.0	9.5	10.9	2.4	3.0	4.4	2.0
	805	14.6	12.4	0.0	13.3	5.4	4.1	9.8	13.8	8.4	10.2
	920	2.8	0.0	12.4	19.4	17.1	13.8	20.2	24.2	22.9	17.0
	1012	0.0	2.8	14.6	20.4	17.9	20.8	25.1	26.4	19.1	16.1
	level										
Scale	102	11.2	13.9	7.4	2.2	3.1	2.4	1.8	3.8	2.0	0.0
C	146	7.8	10.6	4.2	2.9	4.8	4.4	4.8	4.7	0.0	2.0
	208	13.6	15.3	6.2	2.5	4.5	3.8	4.5	0.0	4.7	3.8
	292	11.2	13.4	5.4	2.6	2.8	2.8	0.0	4.5	4.8	1.8
	400	11.8	115.7	6.7	4.4	2.4	0.0	2.8	3.8	14.4	2.4
	530	11.1	12.2	8.4	3.7	0.0	2.4	2.8	4.5	4.8	3.1
	670	10.1	14.0	8.8	0.0	3.7	4.4	2.6	2.5	2.9	2.2
	805	10.4	9.8	0.0	8.8	8.4	6.7	5.4	6.2	4.2	7.4
	920	6.5	0.0	9.8	14.0	12.2	15.7	13.4	15.3	10.6	13.9
	1012	0.0	6.5	10.4	10.1	11.1	11.8	11.2	13.6	7.8	11.2

Table 2.0 **Percentage of alignment of local wind shear with mean-wind shear**

The wind-shear vector computed between 1012mb and 670mb is compared with the direction of the mean wind shear computed between these two levels. The comparison is done for two scale sizes and also for magnitude cut-off of the local wind shear to investigate the variation with it. The percentages of the cases that fall within the ±25, ±35 degrees in the histogram are given in the table. The histogram gives the percentage of cases vs. the angular difference of local wind shear with respect to mean wind shear. The peak angle denotes the angle where the value is highest in the histogram.

magnitude cutoff(m/s)		0	2	4	6	8	10	12
	peak ang.	20°	20°	20°	0°	0°	0°	0°
Scale	±25°	64.8	66.1	76.5	81.5	89.4	94.8	97.3
B/C	±35°	78.1	79.4	88.4	93.2	96.5	99.7	100
	no. cases	1283	1223	977	742	493	308	187
	peak ang.	20°	20°	20°	0°	0°	0°	0°
Scale	±25°	63.7	64.3	71.5	79.8	92.8	95.6	98.2
C	±35°	74.9	75.2	82.2	91.5	97.6	100	100
	no. cases	625	616	507	367	210	153	113

Table 3.0 **Percentage of alignment of local wind shear with linearity vector**

The wind-shear vector computed between 1012mb and 670mb is compared with the cluster directional vector. The comparison is done for two scale sizes and also for the magnitude cut-off of the wind shear to investigate the variation with it. The percentages of the cases that fall within the ±25, ±35 degrees in the histogram are given in the table. The histogram gives the percentage of cases vs. the angular difference of wind-shear with respect to linearity vector. The peak angle denotes the angle where the value is highest in the histogram.

mag cut		0	2	4	6	8	10	12
	peak	0°	0°	0°	0°	0°	0°	0°
Scale	±25°	39.4	39.9	42.7	43.9	47.2	46.4	48.2
B/C	±35°	54.1	54.8	58.3	59.8	62.2	63.0	65.3
	no. cases	1283	1223	977	742	493	308	187
	peak.	20°	20°	10°	10°	10°	10°	10°
Scale	±25°	38.2	38.3	39.9	39.4	42.3	45.7	44.2
C	±35°	51.9	52.1	53.5	54.6	59.4	61.4	60.1
	no. cases	625	616	507	367	210	153	113

Table 4.0 **Percentage of alignment of mean-wind shear with linearity vector**

The direction of the mean-wind shear vector computed between 1012mb and 670mb is compared with the cluster directional vector. The comparison is done for two scale sizes and also for the magnitude cut-off of the local wind shear to investigate the variation with it. The percentages of the cases that fall within the ± 25, ± 35 degrees in the histogram are given in the table. The histogram gives the percentage of cases vs. the angular difference of mean-wind shear vector with respect to linearity vector. The peak angle denotes the angle where the value is highest in the histogram.

magnitude cutoff(m/s)		0	2	4	6	8	10	12
	peak ang.	0°	0°	0°	-	-	0°	0°
Scale	±25°	46.9	46.8	46.1	45.3	48.7	45.4	46.6
B/C	±35°	63.6	63.6	63.1	61.4	65.1	62.3	65.4
	no. cases	1283	1223	977	742	493	308	187
	peak ang.	20°	10°	10°	10°	10°	10°	10°
Scale	±25°	38.8	38.8	37.6	39.0	46.2	47.2	46.0
C	±35°	53.5	53.6	51.4	52.9	58.1	59.6	57.5
	no. cases	625	616	507	367	210	153	113

5.0 SUMMARY AND DISCUSSION

Automated methods were developed to investigate statistical properties of cloud clusters. In this exploratory analysis, we have used simple pattern recognition techniques to identify clusters and their characteristic indices from the radar data estimates of the surface precipitation rates from the ship Gilliss during Phase 3 of GATE. The method identifies cells of enhanced precipitation using a median "high-pass" filter.

Clusters of precipitation cores were identified by single-linkage cluster analysis using the geometric distance between cores as the measure of separation. The statistical characteristics of the clusters identified by the automated method were studied to validate the method and extend the work of previous investigators. The large peaks in the time series of the cluster precipitation were associated with major convective events. The peaks in the time series of widespread precipitation associated with clusters, exhibited a time lag with major cluster precipitation events. This is consistent with case studies of mesoscale convective systems where the anvil precipitation remains for 3 - 12 hours after the peak convective activity (see Houze and Betts, 1981). The total area of cluster cores found by this method showed a good correlation (0.89) with the total precipitation rate. This result is consistent with the work of Short et al (1989), based on a study of raingage and radar data from Australia using a threshold. The automated method was therefore successful in describing many of the known characteristics of cloud clusters.

By studying the characteristics of these clusters several conclusions were drawn. The widespread precipitation as a percentage of total precipitation fluctuated between 100% to 35% with a total average of 64%. Thus a large

proportion of the total precipitation comes from the widespread precipitation. Another interesting conclusion is that the precipitation from large clusters dominates the total precipitation.

It is seen that the area covered by the widespread precipitation had a good correlation with its average precipitation rate with an extremely good second-order fit with a correlation index of 0.97. It could be deduced that this phenomenon is caused by the fact that the large widespread areas would include precipitation cells of higher intensity due to decaying of large clusters. Then again it could be argued that this could be explained by hypothesizing a parabolic structure in the intensity of precipitation where intensity decrease from the center to the periphery.

The relationship between the total precipitation and the widespread area covered was very good with a correlation index of 0.94. Therefore it could be safely argued that if the areal coverage of widespread area is known, then the total precipitation could be estimated to a certain accuracy. This is more or less obvious as the major fraction of the total precipitation is contributed by the widespread areas. The present day satellites posses the capability to identify the widespread areas and thus estimate the total precipitation as explained later in this chapter.

The area of the cluster cores and their precipitation was almost one to one with a correlation of 0.99. With this extremely high correlation the precipitation contribution by the large-scale clusters could be estimated to a very high accuracy. Comparison of time series of number of cores and cluster precipitation suggests that the clusters are made-up of cells of more or less of same intensity. Thus the area of the clusters is a good parameterization factor in evaluating its fractional rainfall contribution to the total within a scan area whose scale size is significantly larger than the convective scale.

An approximately linear relationship with correlation of 0.89 was seen for the total precipitation and the area covered by the cluster precipitation cores. This fact supports the hypothesis that the mesoscale precipitation features are the basic features producing precipitation.

All the above mentioned deductions carry with them important ramifications in parameterization of precipitation and estimation of tropical rainfall from satellite data. For if large clusters could be identified, then the variability in the estimation of the total precipitation could be reduced. Based on our results the most crucial problem for improving satellite precipitation estimates from convective systems is the identification of cluster core area.

Present day satellites (for example the Nimbus type) employ passive microwave measurements of either emission/absorption or scattering for estimation of precipitation. In the emission/absorption regime the radiance from the liquid rain drops are measured and the rainfall is estimated using empirical models. The Scanning Multichannel Microwave Radiometer (SMMR) equipment on the Nimbus-7 has a resolution of about 60km. Thus this low resolution would inhibit the identification of all but the largest clusters. Studies done by Spencer et al (1989) and others for estimating precipitation and height of the clouds using the passive microwave radiation indicate the scope of this method.

In the method using outgoing long-wave measurements, as is done in National Oceanographic and Atmospheric Administration (NOAA) polar orbiter satellite, the cloud top temperature is measured and from this the cloud height is estimated. This measure and the cloud cover is then used to compute the precipitation (see Arkin, 1979). This method is most likely to give widespread area precipitation, but has the inability to gauge the depth of convection and the 3-D structure.

The planned future projects like Tropical Rainfall Measuring Mission (TRMM) are geared to use equipment such as Electronically Scanned Microwave Radiometer (ESMR) with a resolution of 7km, radar with a horizontal resolution of 3km and Advanced Very High Resolution Radiometer (AVHRR) with a resolution of less than 1km. Therefore it is seen that the planned mission will have the capability to resolve mesoscale features by identifying intense precipitation cells and thereby also the clusters. By bringing into the picture the mesoscale organization of clouds, the estimation of the total rainfall over much of the tropics could be improved to a great extent. This would circumvent the need to consider threshold and other questionable methods that are used in the present times. Considering the present day satellite capabilities it is seen that the low resolution would make it somewhat impossible to resolve clusters except very large ones. Even then this method could be tried out as large cells could be identified by the intensity of the precipitation.

We found that the upper-level large-scale vertical motion field around 400mb correlated well with the widespread and total precipitation of which a large fraction is made-up of widespread area precipitation. In these cases the averaged vertical motion was correlated with the widespread area and total precipitation within the scan area. This is additional observational evidence that the anvil area precipitation is accompanied by the mesoscale vertical motion at upper levels, and supports the contention that mesoscale effects must either be resolved or parameterized in large-scale numerical models. A similar upper-level relationship was seen by Houze (1982), where the vertical motion was enhanced in the mature stage of the clusters. This implies that the period when the precipitation rate is highest is accompanied by a higher vertical motion. The correlation also gives observational support to the work

of Kasahara et al (1988). In their scheme, they propose the usage of the Outgoing Longwave Radiation (OLR) to estimate the vertical motion. Higher cloud tops with lower temperature and a higher precipitation rate would imply a correlation of cloud top temperature with vertical motion. In this scheme the satellite radiometric data are used to compute the black body temperature in deep convection areas to estimate the vertical motion which is used to initialize a global prediction model.

The cores which are of convective scale, did not show a strong correlation to the upper-level mesoscale vertical motion field. The lack of correlation is probably due to the difference in the vertical profiles of mass flux in a convective cloud, as well as the time lag between and convective and widespread area precipitation.

Considering all the above mentioned facts it could be stated that the strength of the interactions of the mesoscale vertical motion field with the precipitation makes it important to take them into account in the parameterization of the convection activity for low resolution general circulation.

The correlation of the shear of large-scale horizontal wind with the orientation of the clusters in the horizontal plane was studied. The wind shear between the surface to 670mb showed a better correlation than shear between other levels. This was verified by looking at the probability distribution of angular separation of vectors. The alignment of wind-shear and cluster direction showed a weak statistical relationship. The imperfections in the automated method and other factors such as clusters being in all stages of formation and decay may introduce a certain amount of variation in cluster organization statistics and these may have caused part of this low correlation. Although the statistical relationships are weak, they are consistent with theoretical work by earlier researchers. For example, the model studies of

Dudhia and Moncrief (1987) showed a lower-level wind-shear alignment with the cluster direction. And also in a similar study by Tao and Soong (1986) found that for cases with high Ri number, the low-level tropospheric wind shear played a key role in the alignment of cloud bands. In our study we found that clusters had a better alignment with wind shear and this alignment became closer with the increase in the magnitude of the low-level wind shear. This points to an influence in the evolution and dynamics of the large clusters by the large-scale horizontal wind shear.

The results of this study give observational support to the necessity of considering mesoscale motion in parameterization of cloud effects on momentum, heat and moisture budgets of large-scale atmospheric phenomena.

The automated method that was employed in this study should be used with other independent data sets where different regimes of convection are found and also where the wind-shear profiles are different to that found over GATE area. The results should then be evaluated to generalize the method and all the assumptions made in this study. The automated method was found to be useful as a technique to identify the organization and other characteristics of convection over tropical oceans. This and the many interesting characteristics of the clusters and the related phenomena that this study brought forth suggest that such techniques should be exploited in future work in this area.

REFERENCES

Arakawa, A., and J. Chen, Aug 1986: Closure assumptions in the cumulus parameterization problem. *WMO/IUGG NWP Symposium, Tokyo,* 107-131.

Arkin, P. A., 1979: The relationship between fractional coverage of high cloud and rainfall accumulations during GATE over the B-scale array. *Mon. Wea. Rev.*, **107**, 1382-1387.

Asai, T., 1970: Three-dimensional features of thermal convection in a plane Couette flow. *J. Meteorol. Soc. Japan*, **48**, 18-28.

Atlas, D., D. Rosenfeld and D. A. Short, 1990: The estimation of convective rainfall by area integrals. 1. The theoretical and empirical basis. *J. Geophys. Res.*, **95**, 2153-2160.

Cheng, C. P. and R. A. Houze Jr., 1979: The distribution of convective and mesoscale precipitation in GATE radar echo pattern. *Mon. Wea. Rev.*, **107**, 1370-1381.

Crane, R. K., 1990: Space-time structure of rain rate fields. *J. Geophys. Res.*, **95**, 2011-2020.

Dudhia, J., and M. W. Moncrief, 1987: A numerical simulation of quasi-stationary tropical convective bands. *Quart. J. Roy. Meteorol. Soc.*, **113**, 929-967.

Gamache, J. F., and R. A. Houze, Jr., 1984: Water budget of a mesoscale convective system in the tropics. *J. Atmos. Sci.*, **40**, 1835-1850.

Gower, J. C., and G. J. S. Ross, 1969: Minimum spanning trees and single linkage cluster analysis. *Applied Statistics*, **18**, 54-64.

Houze, R. A.,Jr., 1977: Structure and dynamics of a tropical squall-line system. *Mon. Wea. Rev.*, **105**, 1540-1567.

Houze, R. A.,Jr., 1982: Cloud clusters and large-scale vertical motions in the tropics. *J. Meteorol. Soc. Japan*, **60**, 396-409.

Houze, R. A.,Jr., and C. P. Cheng, 1977: Radar characteristics of tropical convection observed during GATE: Mean properties and trends over the

summer seasons. *Mon. Wea. Rev.*, **105**, 964-980.

Houze Jr., R. A., and A. K. Betts, 1981: Convection in GATE. *Revs. Geophys. Space Phys.*, **19**, No.4, 541-576.

Houze, R. A.,Jr., and E. N. Rappaport, 1984: Air motions and precipitation structure of an early summer squall line over the eastern tropical Atlantic. *J. Atmos. Sci.*, **41**, 553-574.

Houze Jr., R.A., B. F. Smull, and Peter Dodge, 1990: Mesoscale organization of springtime rainstorms in Oklahoma. *Mon. Wea. Rev.*, **118**, 613-654.

Kasahara, A., R. C. Balgovind, and B. B. Katz, 1988: Use of satellite radiometric imagery data for improvement in the analysis of divergent wind in the tropics. *Mon. Wea. Rev.*, **116**, 866-883.

Kessler, E., 1969: On the distribution and continuity of water substance in atmospheric circulation. *Meteor. Monogr., No 32*, Amer. Meteor Soc.,84 pp.

Leary, C. A., and R. A. Houze Jr., 1980: The contributions of the mesoscale motions to mass and heat fluxes of an intense tropical convective system. *J. Atmos. Sci.*, **37**, 784-796.

Leary, C. A., 1984: Precipitation structure of cloud clusters in a tropical easterly wave. *Mon. Wea. Rev.*, **112**, 313-325.

Lopez, R. E., 1978: Internal structure and development processes of C-scale aggregate of cumulus clouds. *Mon. Wea. Rev.*, **106**, 1488-1494.

Malkus, J. S. and H. Riehl, 1964: *Cloud structure and Distributions over the Tropical Pacific Ocean.* University of California Press, Berkeley and Los Angeles, 229 pp.

Miller, M. J., and R. P. Pearce, 1974: A three-dimensional primitive equation model of cumulonimbus convection. *ibid.*, **100**, 133-154.

Moncrieff, M. W., and M. J. Miller, 1976: The dynamics and simulation of tropical cumulonimbus and squall lines. *Quart. J. Roy. Meteorol. Soc.*, **102**, 373-394.

Neter J., W. Wasserman and M. H. Kutner, 1985: Applied linear statistical models. *2nd Edition, ISBN No. 0 - 256 - 02447 - 2*

Ooyama, K. V., 1985: The polar representation of tensor cross-spectra of winds. *16th Conference on Hurricanes and Tropical Meteorology, May 14-17, 1985, Houstan, Texas* 182-183.

Ooyama, K. V., 1987: Scale-controlled objective analysis. *Mon. Wea. Rev.*, **115**, 2479-2506.

Patterson, V. L., M. D. Hudlow, P. J. Pytlowany, F. P. Richards and J. D. Hoff, May 1979: GATE radar rainfall processing system. *NOAA Technical Memorandum EDIS 26.*

Raghavan, S., T. R. Sivaramakrishnan and B. Ramakrishnan, 1983: Size distribution of radar echoes as an indicator of growth mechanisms in Monsoon clouds around Madras. *J. Atmos. Sci.*, **40**, 428-434.

Ramirez, J. A., R. L. Bras, 1990: Clustered or regular cumulus cloud fields: The statistical character of observed and simulated cloud fields. *J. Geophys. Res.*, **95**, 2035-2045

Rogers R. R., 1979: A short course in cloud physics. *2nd Edition ISBN No. 0-08-023040-7 pp 179-193*

Short, D. A., D. Rosenfeld, D. B. Wolff and D. Atlas, 1989: A raingage, radar and satellite simulation study of the estimation of convection rainfall by area-time integrals. *Fourth Conference on Satellite Meterology and Oceanography : May 1989, San Diego, Calif.*, 90-94.

Spencer, R. W., H. M. Goodman and R. E. Hood, 1989: Precipitation retrieval over land and ocean with the SSM/I: Identification and characteristics of the scattering signal. *J. Atmos. Ocea. Techno.*, **6**, 254-273.

Sun, W. Y., 1978: Stability analysis of deep cloud streets - Part 1.*J. Atmos. Sci.*, **35**, 466-483.

Szoke, E. J., and E. J. Zipser, 1986: A radar study of convective cells in mesoscale systems in GATE. Part 1: Vertical profile statistics and comparison with hurricanes. *J. Atmos. Sci.*, **43**, 182-197.

Szoke, E. J., and E. J.and Zipser, 1986: A radar study of convective cells in mesoscale systems in GATE. Part 2: Life cycles of convective cells. *J. Atmos. Sci.*, **43**, 199-218.

Tao, W. K., and S. T. Soong, 1986: A study of the response of deep tropical clouds to mesoscale processes: Three-dimensional numerical experiment.

J. Atmos. Sci., **43**, 2653-2676.

Tollerud, E. I., and S. K. Esbensen, 1985: A composite life cycle of nonsquall mesoscale convective systems over the tropical ocean. Part 1: Kinematic fields. *J. Atmos. Sci.*, **42**, 823-837.

Warner, C., J. Simpson and G. Van Helvoint, 1980: Deep convection on day 261 of GATE. *Mon. Wea. Rev.*, **108**, 169-194.

Zipser, E. J., R. J. Meitin and M. A. LeMone, 1981: Mesoscale motion fields associated with a slowly moving GATE convective band. *J. Atmos. Sci.*, **38**, 1725-1750.

APPENDICES

APPENDIX A

1.0 The parameters for computation.

(a) Total rainfall rate : TRR = Σ RRT

where RRT - rainfall rate per box

(b) Average rainfall rate per scan :

ARR = ΣRRT/(scan area)

(c) Linearity measure : L = LLGTH/SLGTH - 1.0

LLGTH - long length of the side of the cluster box.

SLGTH - short length of the side of the cluster box.

APPENDIX B

1.0 The tensor correlation of wind-shear and linearity vectors

The method that is used in this analysis is given below. The wind-shear vector at the 'i'th level with respect to 'j'th level and the linearity vector such that it makes an acute angle with the wind-shear is:

$$\underset{\sim}{\mathrm{U}}'_{i(j)} = \begin{bmatrix} u_i - u_j \\ v_i - v_j \end{bmatrix} = \begin{bmatrix} u_{i(j)} \\ v_{i(j)} \end{bmatrix} \text{ and } \underset{\sim}{\mathrm{L}}'_{i(j)} = \begin{bmatrix} x_{i(j)} \\ y_{i(j)} \end{bmatrix}$$
$$i = 1, n; \qquad (1.1)$$
$$i \neq j$$
where n is the number of height levels.

For each wind-shear and linearity vector for a particular level, as defined above an associate vector is introduced that is equal in magnitude but opposite in direction. This will keep the orientation of the vectors to each other intact but will reduce the mean of the vectors to zero. Thus the correlation will be that between wind-shear and linearity vectors rather than between their deviations from some mean. Therefore,

$$\underset{\sim}{\mathrm{U}}_{i(j)} = \underset{\sim}{\mathrm{U}}'_{i(j)} - \langle \underset{\sim}{\mathrm{U}}'_{i(j)} \rangle = \underset{\sim}{\mathrm{U}}'_{i(j)}$$
$$\qquad (1.2)$$
$$\underset{\sim}{\mathrm{L}}_{i(j)} = \underset{\sim}{\mathrm{L}}'_{i(j)} - \langle \underset{\sim}{\mathrm{L}}'_{i(j)} \rangle = \underset{\sim}{\mathrm{L}}'_{i(j)}$$

Thus the covariance tensor element for wind shear for the 'i'th level with reference to the 'j'th level is defined in terms of the Cartesian components by:

$$\hat{\underset{\sim}{\mathrm{m}}}_{ii(j)} = \langle \underset{\sim}{\mathrm{U}}_{i(j)} \underset{\sim}{\mathrm{L}}_{i(j)} \rangle$$
$$= \begin{bmatrix} \langle u_{i(j)} x_{i(j)} \rangle & \langle u_{i(j)} y_{i(j)} \rangle \\ \langle v_{i(j)} x_{i(j)} \rangle & \langle v_{i(j)} y_{i(j)} \rangle \end{bmatrix} \qquad (1.3)$$

Thus the covariance tensor for the n-levels with reference to the 'j' level is:

$$M_{(j)} = (\hat{\underset{\sim}{m}}_{ik(j)} \delta_{ik})_{n \times n}$$

$$i \neq j \tag{1.4}$$

$$\text{where } \delta_{ik} = \begin{cases} 1 & \text{i= k} \\ 0 & i \neq k \end{cases}$$

For the tensor covariance to be interpreted it is necessary to normalize it by the tensor variances of the vector data thus preserving the invariant properties.

The variance tensor of wind-shear at the 'i'th level with respect to the 'j'th level is given by:

$$[\hat{\underset{\sim}{S}}_{u(j)}]^2 = [\hat{\underset{\sim}{s}}_{u^2_{ik(j)}} \delta_{ik}]_{n \times n}$$

$$i \neq j \tag{1.5}$$

$$\text{where, } \hat{\underset{\sim}{s}}_{u^2_{ii(j)}} = \langle \underset{\sim}{U}_{i(j)} \underset{\sim}{U}^T_{i(j)} \rangle$$

The square-root of the variance tensor and its inverse is also a tensor; computational methods are discussed in Sec.2.0

Therefore for wind shear (computed with reference to 'j'th level) the square-root of the variance tensor and its inverse is defined as:

$$[\hat{\underset{\sim}{S}}_{u(j)}] = [\hat{\underset{\sim}{s}}_{u_{ik(j)}} \delta_{ik}]_{n \times n}$$

$$i \neq j$$

$$[\hat{\underset{\sim}{S}}_{u(j)}]^{-1} = [\hat{\underset{\sim}{s}}_{u^{-1}_{ik(j)}} \delta_{ik}]_{n \times n} \tag{1.6}$$

$$i \neq j$$

Similarly, the inverse of the linearity vector is:

$$[\hat{\underset{\sim}{S}}_{l(j)}]^{-1} = [\hat{\underset{\sim}{s}}_{l^{-1}_{ik(j)}} \delta_{ik}]_{n \times n} \tag{1.7}$$

$$i \neq j$$

Therefore normalizing the covariance tensor by the inverse of square-

root of the variance tensors of linearity and wind-shear :

$$N_{(j)} = [\hat{\underset{\sim}{S}}_{u_{(j)}}]^{-1} [M_{(j)}] [\hat{\underset{\sim}{S}}_{l_{(j)}}]^{-1}$$
$$\text{where, } [\hat{\underset{\sim}{N}}_{(j)}] = [\hat{\underset{\sim}{n}}_{ik(j)} \delta_{ik}]_{\substack{n \times n \\ i \neq j}} \tag{1.8}$$

Thus it is seen that the normalized covariance tensor is a diagonal matrix with each element made-up by a 2×2 Cartesian tensor. This procedure was repeated by varying the 'j' reference level which is used as a reference to compute the wind shear at other levels. From now on 'j' subscript will be dropped for simplicity.

The 2×2 Cartesian tensor elements thus obtained by normalizing the covariance tensor is represented in polar form (see Sec.3.0) by separating it into two parts, one which is invariant to coordinate rotation (called scalar or axial scalar part), and the other which must transform with rotation (called irreducible tensor part).

Therefore,

$$\hat{\underset{\sim}{n}}_{ii} \quad = \quad S_i \, \underset{\sim}{l}(\alpha_i) \quad + \quad T_i \, \underset{\sim}{d}(\tau_i) \tag{1.9}$$

Where $\underset{\sim}{l}(\alpha_i)$ and $\underset{\sim}{d}(\tau_i)$ as defined in Sec.3.0.

Si measures the magnitude of the scalar part which measures the correlation while α_i measures the relative angle by which the wind shear is statistically ahead (measured CCW) of linearity. Ti measures the irreducible part which gives the stretching of the covariance in the direction of angle τ_i. This gives a somewhat preferential geographical direction for which the correlation between the vectors is highest.

2.0 The square root and it's inverse of a tensor.

The method given below is based on Ooyama (1987). The variance

tensor is given by :

$$[\hat{\underset{\sim}{S}}^2] = (\hat{s}^2_{ik}\delta_{ik})_{n\times n} \tag{2.1}$$

As an example, for wind shear (computed with respect to 'j'th level) the (i,i)th element of the variance tensor is :

$$\hat{s}_{u^2_{ii(j)}} = \langle \underset{\sim}{U}_{i(j)} \underset{\sim}{U}_{i(j)} \rangle = \begin{pmatrix} \langle u_{i(j)} u_{i(j)} \rangle & \langle u_{i(j)} v_{i(j)} \rangle \\ \langle u_{i(j)} v_{i(j)} \rangle & \langle v_{i(j)} v_{i(j)} \rangle \end{pmatrix}$$

$$= \begin{pmatrix} A & C \\ C^* & B \end{pmatrix} \tag{2.2}$$

(say and for real quantities C = C*)

Then let,

$$\begin{aligned} D &= (AB - CC^*)^{1/2} \\ X &= (A + B + 2D)^{1/2} \\ a &= \frac{1}{2}\left(X + \frac{A-B}{X}\right) \\ b &= \frac{1}{2}\left(X - \frac{A-B}{X}\right) \\ c &= \frac{C}{X} \end{aligned} \tag{2.3}$$

Then the square-root for the variance tensor element is a positive definite matrix given by :

$$\hat{s}_{u_{ii(j)}} = \begin{pmatrix} a & c \\ c^* & b \end{pmatrix}$$

and it's inverse is (2.4)

$$\hat{s}_{u^{-1}_{ii(j)}} = \frac{1}{D}\begin{pmatrix} b & -c \\ -c^* & a \end{pmatrix}$$

Thus the inverse of the square-root of variance tensor is given by:

$$[\hat{\underset{\sim}{S}}]^{-1} = (\hat{s}_{u^{-1}_{ik}}\delta_{ik})_{n\times n} \tag{2.5}$$

3.0 Polar representation of tensor cross-spectra

The following derivation is based on Ooyama (1985) and it explains the method of decomposing a tensor element made-up of 2 × 2 matrix of Cartesian components, into two parts. One that is invariant to co-ordinate rotation called the scalar or the axial scalar part and the other that must transform with the rotation called the irreducible tensor part.

$$\underset{\sim}{n} = S\,\underset{\sim}{l}(\alpha) + T\,\underset{\sim}{d}(\tau) \tag{3.1}$$

where,

$$\underset{\sim}{n} = \text{Cartesean tensor element} : \begin{pmatrix} n_{11} & n_{12} \\ n_{21} & n_{22} \end{pmatrix}$$

$$\underset{\sim}{l}(\alpha) = \begin{pmatrix} \cos(\alpha) & -\sin(\alpha) \\ \sin(\alpha) & \cos(\alpha) \end{pmatrix}$$

$$\underset{\sim}{d}(\tau) = \underset{\sim}{l}(\tau) \begin{pmatrix} 1 & 0 \\ 0 & -1 \end{pmatrix} \underset{\sim}{l}(-\tau)$$

substituting,

$$\underset{\sim}{d}(\tau) = \begin{pmatrix} \cos(\tau) & -\sin(\tau) \\ \sin(\tau) & \cos(\tau) \end{pmatrix} \begin{pmatrix} 1 & 0 \\ 0 & -1 \end{pmatrix} \begin{pmatrix} \cos(\tau) & \sin(\tau) \\ -\sin(\tau) & \cos(\tau) \end{pmatrix}$$

$$= \begin{pmatrix} \cos(2\tau) & \sin(2\tau) \\ \sin(2\tau) & -\cos(2\tau) \end{pmatrix}$$

thus,

$$\begin{pmatrix} n_{11} & n_{12} \\ n_{21} & n_{22} \end{pmatrix} = S \begin{pmatrix} \cos(\alpha) & -\sin(\alpha) \\ \sin(\alpha) & \cos(\alpha) \end{pmatrix} + T \begin{pmatrix} \cos(2\tau) & \sin(2\tau) \\ \sin(2\tau) & -\cos(2\tau) \end{pmatrix}$$

solving the system,

$$\begin{aligned} S\cos(\alpha) &= \frac{1}{2}(n_{11}+n_{22}) = S_1 \\ S\sin(\alpha) &= \frac{1}{2}(n_{21}-n_{12}) = S_2 \\ T\cos(2\tau) &= \frac{1}{2}(n_{11}-n_{22}) = T_1 \\ T\sin(2\tau) &= \frac{1}{2}(n_{12}+n_{21}) = T_2 \end{aligned}$$

therefore,

$$\begin{aligned} S &= \left({S_1}^2 + {S_2}^2\right)^{\frac{1}{2}} \text{ and } T = \left({T_1}^2 + {T_2}^2\right)^{\frac{1}{2}} \text{ and} \\ \alpha &= \arccos\left(\frac{S_1}{S}\right) = \arcsin\left(\frac{S_2}{S}\right) \\ \tau &= \frac{1}{2}\arccos\left(\frac{T_1}{T}\right) = \frac{1}{2}\arcsin\left(\frac{T_2}{T}\right) \end{aligned} \tag{3.2}$$